increased frequency of unciliated cells, and infiltration of inflammatory cells and erythrocytes upon ΔBopN infection (Fig. 3 B, arrows). To eliminate the possibility that BopN is involved in the cytotoxic phenotype, DC2.4 cells were infected with *Bordetella* and examined under a light microscope (Fig. 3 C). In addition, we measured the release of lactate dehydrogenase (LDH) into the extracellular medium from the infected cells (Fig. 3 D). ΔBopC and ΔT3SS (unpublished data) elicited no cytotoxicity in the infected DC2.4 cells. In contrast, infection with WT or ΔBopN produced

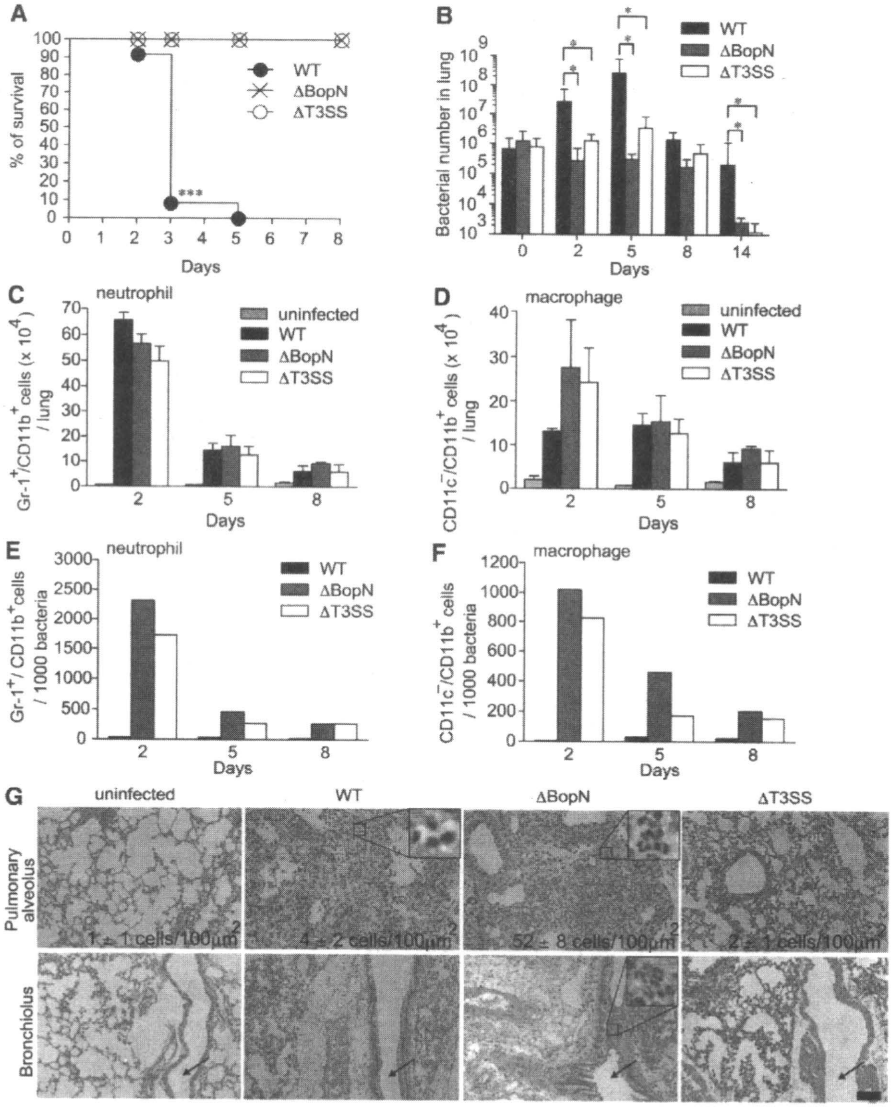

Figure 2. BopN is required for disease process. (A) C57BL/6J mice (n = 27 for each group) were infected intranasally with 5×10^6 *B. bronchiseptica* WT, ΔbopN, or ΔT3SS, and the survival was monitored for 8 d after infection. ***, $P < 0.0001$ using the log-rank test. (B) Mice (n = 15 for each group) infected intranasally with the specified strains (5×10^5 bacteria) were sacrificed at the indicated days after infection. Lung specimens were homogenized and plated on BG agar plates. Colonies were counted to determine the number of colonized bacteria per lung. The values are means ± SD from three independent experiments. *, $P < 0.05$. (C and D) Mice (n = 9 for each group) infected intranasally with the indicated strains (5×10^5 bacteria) were sacrificed, and cells were isolated from the whole lung. The total numbers of neutrophils (C) or macrophages (D) in the lung were determined by FACS analysis. The values are means ± SE from three independent experiments. *, $P < 0.05$. (E and F) The total number of neutrophils or macrophages in the lung obtained from C or D, respectively, was normalized by the bacterial number in the lung obtained from B. The values are means ± SE from three independent experiments. (G) 2 d after infection (5×10^5 bacteria), lung sections were fixed and stained with H&E. The infiltration of neutrophils and macrophages into the pulmonary alveoli and peribronchiolar edema formation are observed in mice infected with WT, ΔbopN, and ΔT3SS. Arrows indicate bronchioles. The number of neutrophils per 100 μm² was determined in three randomly obtained images of pulmonary alveoli. The area of the enlarged boxes corresponds to 8 μm². Bar, 100 μm.

similar cytotoxic effects, indicating that BopN is not involved in the cytotoxic phenotype. These results are consistent with the hypothesis that BopN functions as an immunosuppressive modulator to down-regulate the host inflammatory responses. Thus, *Bordetella* has the ability to alter the tracheal microenvironment for its own benefit by exploitation of BopN.

Up-regulation of IL-10 benefits *Bordetella*

We have clearly demonstrated that BopN is involved in the up-regulation of IL-10 in infected DC2.4 cells (Fig. 1) and that this effector is an essential virulence factor that subverts the host immune system (Fig. 2 and Fig. 3). To further investigate the role of BopN in vivo, mice were infected intranasally

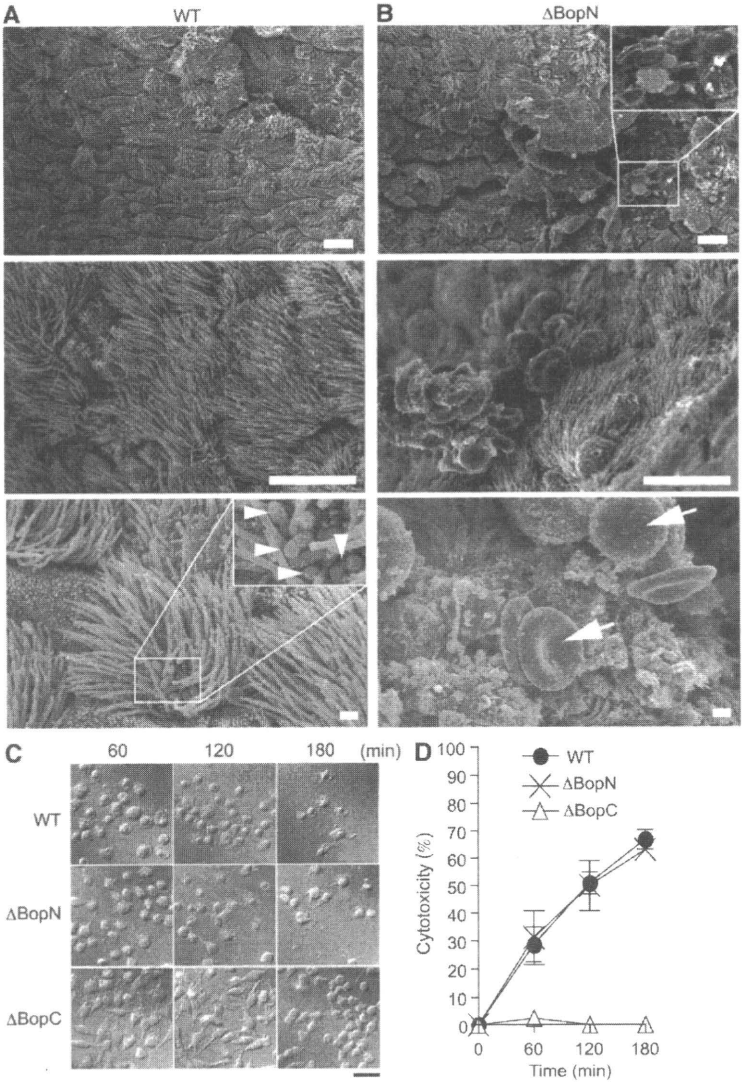

Figure 3. BopN suppresses inflammatory responses at the bacterial-colonized area. (A and B) Scanning electron micrographs of mouse tracheas infected with WT (A) and ΔBopN *Bordetella* (B). C57BL/6J mice were infected intranasally with 5×10^6 WT and ΔBopN *B. bronchiseptica*, and tracheal sections were obtained 2 d after infection. Arrowheads indicate bacteria. Arrows indicate erythrocytes and inflammatory cells. Note that extensive cell-surface disruption, including increased unciliated cells as well as infiltration of inflammatory cells and erythrocytes, is observed in mice infected with ΔBopN but not WT. The areas of the enlarged boxes correspond to 20 μm^2 (top) and 4 μm^2 (bottom). Bars: (top and middle) 10 μm; (bottom) 1 μm. (C) DC2.4 cells were infected with the indicated strains (m.o.i. = 10) for 60, 120, and 180 min and then analyzed with Nomarski imaging. Both WT and ΔBopN induced significant morphological changes, including rounding and detachment, in the cells. Bar, 20 μm. (D) Time course of the release of LDH into the extracellular medium from DC2.4 cells infected with the indicated strains. The values are the percentages of LDH released from Triton X-100–lysed DC2.4 cells after subtraction of the value measured in uninfected cells. Error bars represent means ± SE from triplicate experiments. The amounts of LDH released after ΔBopN infection were similar to those released after WT infection.

with WT *B. bronchiseptica* or a mutant strain, and the amounts of the cytokine produced were determined by ELISA on homogenized lung specimens (Fig. 4, A and B). The production of the antiinflammatory cytokine IL-10 in the lungs of mice infected with WT was significantly higher than that in the lungs of mice infected with ΔBopN or ΔT3SS on day 2 or 5 (Fig. 4 A). In contrast, the production of the inflammatory cytokine IFN-γ in mice infected with WT was significantly lower than that of mice infected with ΔBopN or ΔT3SS (Fig. 4 B). These results clearly indicate that BopN is involved in the up-regulation of IL-10 production in vivo, thereby leading to the inhibition of IFN-γ production.

To further investigate whether the major biological target of BopN in the pathophysiology of *Bordetella* infection is the up-regulation of IL-10, WT and IL-10$^{-/-}$ mice were infected intranasally with WT or ΔBopN *B. bronchiseptica*. As expected (Skinner et al., 2005), WT *Bordetella* colonization in IL-10$^{-/-}$ mice was significantly decreased compared with that in C57BL/6J mice 2 d after infection (Fig. 4 C). Importantly, although the colonization by WT *Bordetella* was significantly higher than that of ΔBopN in C57BL/6J mice, no significant difference was found between WT and ΔBopN colonization in IL-10$^{-/-}$ mice (Fig. 4 C). In addition, although the production of IFN-γ in the lungs of C57BL/6J mice infected with WT *Bordetella* was significantly lower than that of mice infected with ΔBopN, no significant difference was found comparing WT and ΔBopN infection in IL-10$^{-/-}$ mice; large amounts of IFN-γ were produced in the lungs of IL-10$^{-/-}$ mice upon infection with either WT or ΔBopN (Fig. 4 D). This genetic evidence indicates that the major in vivo target of BopN is indeed the regulation of IL-10 production and that BopN exploits IL-10 to establish persistent colonization during *Bordetella* infection.

CD11c$^+$ cells are recruited into pulmonary alveoli during *Bordetella* infection

IL-10 production by DCs and macrophages is essential for the control of excessive inflammatory responses. Our study demonstrated that the disease process of *Bordetella* infection involves the function of BopN in IL-10 up-regulation. To further confirm whether *Bordetella* exploits IL-10–producing cells during infection, we performed immunostaining on lung sections obtained from mice infected with WT or ΔBopN *Bordetella*. Immunostaining for CD11c, one of the main surface antigens present in DCs or macrophages (Fig. 5 A), showed extensive recruitment of CD11c$^+$ cells into the pulmonary alveoli of WT *Bordetella*-infected lung tissues. A similar observation was obtained using ΔBopN-infected tissue, suggesting that the absence of BopN does not affect CD11c$^+$ cell recruitment to the lung. We also determined the number of CD11c$^+$ cells in the lung by FACS analysis (Fig. 5 B). Again, the total number of CD11c$^+$ cells in the

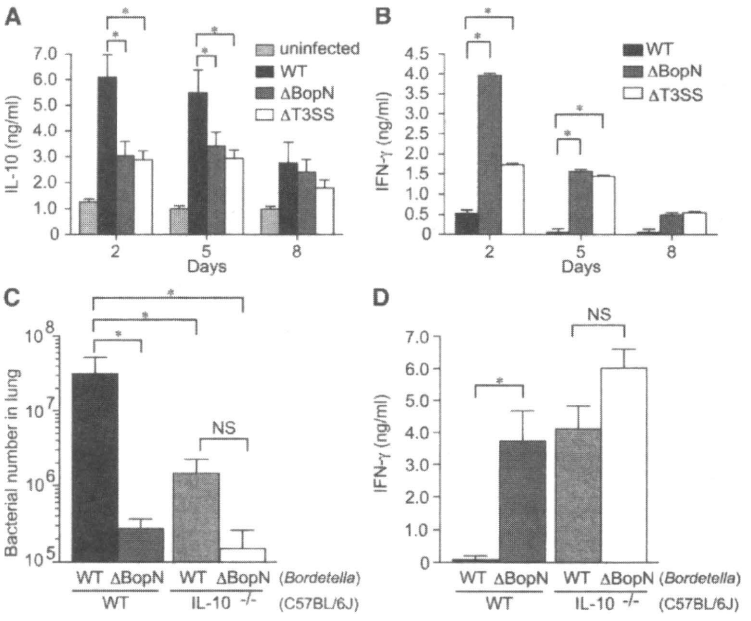

Figure 4. BopN induces IL-10 production in vivo. (A and B) Detection of IL-10 (A) or IFN-γ (B) production in *Bordetella*-infected mice is shown. C57BL/6J mice (n = 9 for each group) were infected intranasally with 5 × 10^5 *B. bronchiseptica*. Homogenized lung specimens were prepared from mice infected with the indicated strains at 2, 5, or 8 d after infection, and the amounts of cytokines in the specimens were determined by ELISA. (C) C57BL/6J (WT) or IL-10$^{-/-}$ mice (n = 3 for each group) on a C57BL/6J background were infected intranasally with the indicated strains (5 × 10^5 bacteria). 2 d after infection, lung specimens were homogenized and plated on BG agar plates to detect the number of colonizing bacteria. (D) IFN-γ production in the lungs of *Bordetella*-infected mice (n = 3 for each group). Homogenized lung specimens were prepared and the amounts of cytokines were determined by ELISA. The values are means ± SE from three independent experiments. *, $P < 0.05$.

lung of mice infected with WT was similar to that in the lung of mice infected with ΔBopN (Fig. 5 B). However, the percentage of IL-10$^+$ CD11c$^+$ cells in the lung upon WT infection was significantly higher than that in the lung upon ΔBopN infection (Fig. 5, C and D). Collectively, these results indicate that *Bordetella* allows recruitment of CD11c$^+$ cells during infection, thus leading to the up-regulation of IL-10 production by BopN.

Preinfection with ΔBopN allows mice to survive a lethal dose of *Bordetella*

Our in vitro and in vivo data led us to hypothesize that if mice were pretreated with ΔBopN, which allows strong host inflammatory responses, they might be able to survive a subsequent lethal dose of *Bordetella* WT bacteria. Hence, we performed a successive infection study (Fig. 6). C57BL/6J mice were infected intranasally with ΔBopN (5×10^5 bacteria) or PBS (mock preinfection) 24 h before WT *Bordetella* infection (9×10^5 bacteria). As shown in Fig. 6 A, although all mice with mock preinfection were killed by a lethal dose of WT bacteria, 24 out of 27 mice preinfected with ΔBopN survived the WT infection. The in vivo successive infection study clearly demonstrates that preinduction of host inflammatory responses by an avirulent ΔBopN strain contributes to survival of the mice upon a lethal dose of WT *Bordetella*. Indeed, the number of bacteria in the lung was greatly decreased by the ΔBopN preinfection (Fig. 6 B). Furthermore, the up-regulation of IL-10 production by WT *Bordetella* was disturbed by preinfection with ΔBopN (Fig. 6 C), and the production of IFN-γ in mice preinfected with ΔBopN was significantly higher than that of mice undergoing mock preinfection (Fig. 6 D). Collectively, these results confirm that the up-regulation of IL-10 by the BopN effector, resulting in the suppression of IFN-γ signaling, is a significant stealth strategy by which *Bordetella* evades the host immune system.

BopN regulates the mitogen-activated protein kinase (MAPK) signaling pathways

Infection with *B. bronchiseptica* triggers the down-regulation (dephosphorylation) of MAPKs (Reissinger et al., 2005) in a T3SS-dependent manner. To examine whether the BopN effector is involved in MAPK signaling alterations, we assessed MAPK signaling in DC2.4 cells infected with *Bordetella* by immunoblot analysis using phosphospecific anti-p38, anti–extracellular signal-regulated kinase (ERK) 1 and –ERK2, or anti–c-Jun N-terminal kinase (JNK) antibodies (Fig. 7 A). Band intensities of the phosphorylated and total MAPK products were quantified using the ImageJ application (Fig. S2 A). At 30 min after infection, the amounts of phospho-p38 in DC2.4 cells infected with WT were significantly lower than those in DC2.4 cells infected with ΔBopN or ΔT3SS. Similarly, the level of phosphorylated (active)

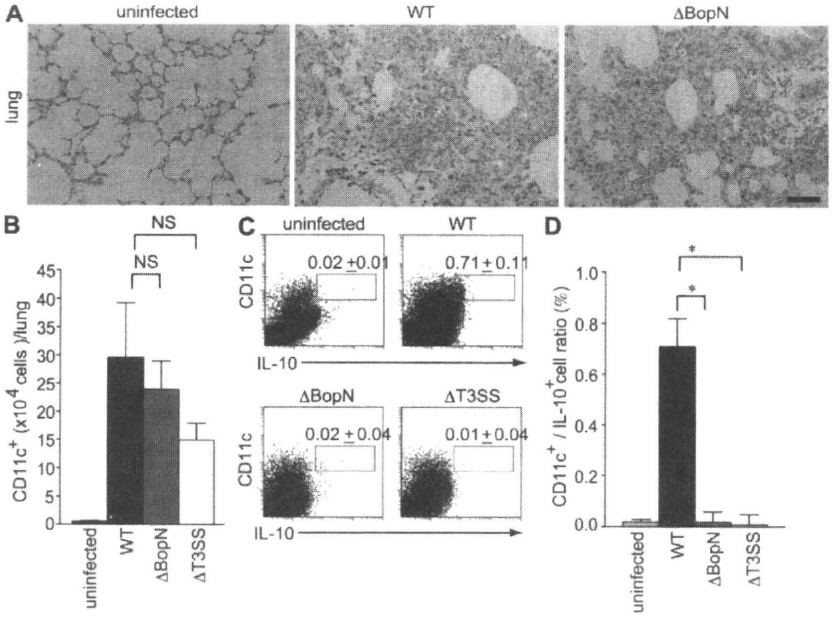

Figure 5. CD11c$^+$ cells migrate into the lung and produce IL-10 during *Bordetella* infection. (A) C57BL/6J mice were infected intranasally with 5×10^5 WT or ΔBopN *B. bronchiseptica*. 2 d after infection, lung sections were immunostained with anti-CD11c monoclonal antibodies (brown). Note that extensive recruitment of CD11c$^+$ cells into the pulmonary alveoli was observed in mice infected with WT and ΔBopN. Bar, 50 μm. (B) 2 d after infection, the total numbers of CD11c$^+$ cells in the lungs of mice ($n = 3$ for each group) infected with the indicated strains were determined by FACS analysis. (C) The lung cells from mice ($n = 3$ for each group) infected with *Bordetella* were pooled, stained with FITC-conjugated anti–IL-10 and PE-conjugated anti-CD11c, and determined by FACS analysis (percentages are shown). (D) The histogram shows the results obtained in C expressed as a ratio of IL-10$^+$/CD11c$^+$ cells. The values in B and D are means ± SE from three independent experiments. *, $P < 0.05$.

ERK2 and JNK in DC2.4 cells infected with WT was lower than that in ΔBopN or ΔT3SS (Fig. 7 A and Fig. S2 A). To further confirm the down-regulation of MAPK signaling by BopN, we assessed the subcellular localization of ERK after *Bordetella* infection and compared the localization of total ERK with that of active phosphorylated ERK (Fig. 7 B). The specificity of phospho-ERK antibodies was also confirmed by pretreatment of cells with a specific MEK1/2 inhibitor, U0126 (Fig. S2 B). In addition, we determined the percentages of cells showing phosphorylated ERK (Fig. S2 C). The number of cells showing phosphorylated ERK was significantly decreased in WT infection relative to ΔBopN infection. These results clearly indicate that BopN is involved in the down-regulation of MAPKs. To examine the relationship between the down-regulation of MAPKs and IL-10 production, MAPK inhibitors were used (Fig. 7 C). Inhibition of the p38 pathway with a specific inhibitor, SB203580, did not greatly affect the level of IL-10 mRNA expression. However, the level of IL-10 mRNA was significantly increased in DC2.4 cells infected with ΔBopN when DCs were treated with the specific MEK1/2 inhibitor U0126 (Fig. 7 C). We assessed the activity of the MEK1/2 and MKK3/MKK6 signaling by immunoblotting (Fig. 7 D). The amounts of phospho-MEK1/2 and phospho-MKK3/MKK6 in DC2.4 cells infected with WT were lower than those in DC2.4 cells infected with ΔBopN or ΔT3SS (Fig. 7 D).

To characterize the transcription factors affected by BopN, nuclear extracts were prepared from DC2.4 cells infected with WT, ΔbopN, and ΔT3SS *Bordetella*, and transcription factor activities were analyzed using a Multiplex transcription factor profiling kit. The level of AP-1 and CREB activation in DC2.4 cells was significantly reduced after infection with WT relative to ΔBopN infection (Fig. 7 E). These observations were consistent with the fact that MAPK signaling is down-regulated by the function of BopN, because both AP-1 and CREB transcription factors are downstream of MAPKs. Collectively, BopN down-regulates both MAPK kinase and MAPK signaling pathways.

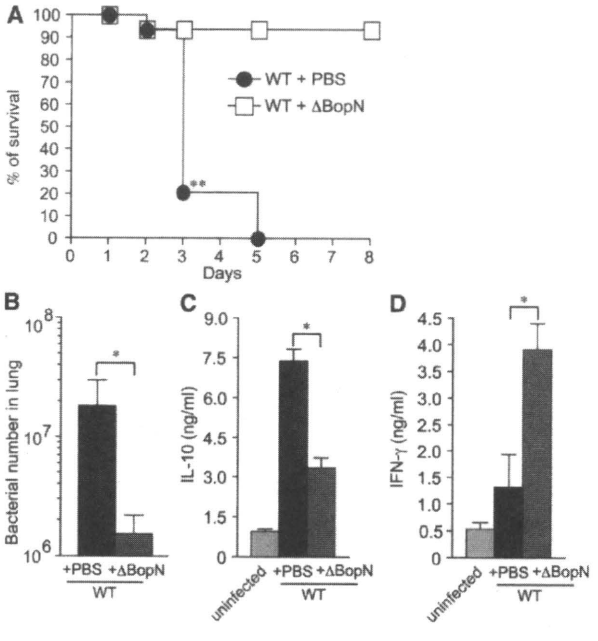

Figure 6. In vivo successive infection study. (A) C57BL/6J mice (n = 27 for WT + PBS and WT + ΔBopN) were infected intranasally with 5×10^5 ΔBopN or PBS (mock infection) 24 h before infection with a lethal dose of WT *Bordetella* (9×10^5), and the survival was monitored for 8 d. **, $P < 0.005$ using the log-rank test. (B) 2 d after the WT lethal-dose infection, the lung specimens of mice (n = 3 for WT + PBS preinfection and WT + ΔBopN preinfection) were homogenized and plated on BG agar plates to detect the number of colonized bacteria. (C and D) 2 d after the WT lethal-dose infection, homogenized lung specimens were prepared from mice (n = 3 for WT + PBS and WT + ΔBopN) infected with the indicated strains, and the amount of IL-10 (C) or IFN-γ (D) in the specimen was determined by ELISA. The values in B–D are means ± SD from three independent experiments. *, $P < 0.05$.

BopN regulates the NF-κB signaling pathways

It has also been reported that NF-κB pathways are modulated during *B. bronchiseptica* infection (Yuk et al., 2000). Therefore, the translocation of NF-κB into the nucleus was investigated using DC2.4 cells infected with *Bordetella*. DC2.4 cells were infected with WT or ΔBopN for 20 min and then fixed and permeabilized. NF-κB translocation was analyzed by immunofluorescence microscopy using anti–NF-κBp65 or anti–NF-κBp50 antibodies (Fig. 8, A and B). As expected (Yuk et al., 2000), the translocation of NF-κBp65 into nuclei was inhibited by WT *B. bronchiseptica* infection (Fig. 8 A). In contrast, the nuclear translocation of NF-κBp65 was intact in the absence of BopN (Fig. 8 A, ΔBopN). The difference in NF-κBp65 translocation into nuclei between WT and ΔBopN infection was statistically significant (Fig. 8 C). Conversely, the nuclear translocation of NF-κBp50 observed after WT infection was significantly blocked in the absence of BopN (Fig. 8, B and C). To further confirm the subcellular distribution of NF-κB, DC2.4 cells infected with *Bordetella* for 30 min were separated into nuclear and cytosolic fractions. The resulting fractions were subjected to immunoblot analysis using anti–NF-κBp65 and anti–NF-κBp50 antibodies (Fig. 8 D). NF-κBp65 translocation into nuclei was greatly inhibited by WT *Bordetella* infection. In contrast, NF-κBp65 was detected in the nuclear fraction of DC2.4 cells infected with ΔBopN or ΔT3SS. Conversely, the nuclear translocation of NF-κBp50 observed after WT infection was largely blocked in the absence of BopN (Fig. 8 D). Thus, BopN participates in altering the nuclear compartmentalization of NF-κB p65 and p50 subunits.

Inhibition of inhibitor of NF-κB (IκB) degradation by a bacterial effector is one bacterial strategy to prevent NF-κB translocation into nuclei (see Discussion). To determine if BopN is involved in the inhibition of IκB degradation, DC2.4 cells were stimulated with 10 μg/ml LPS or infected with WT, ΔBopN, and ΔT3SS *B. bronchiseptica*, and the cell lysates were analyzed using immunoblotting with anti-IκBα,

anti-IκBβ, anti-IκBε, and anti–NF-κBp105 antibodies (Fig. 8 E). Degradation of IκBα was detected in DC2.4 cells infected with WT and ΔBopN *B. bronchiseptica*. In contrast, degradation of IκBβ, IκBε, and NF-κBp105 was not detected during *Bordetella* infection. Thus, IκBα degradation is triggered by *Bordetella* infection, but this event is independent of BopN function.

To investigate whether the nuclear export of proteins, such as NF-κB, is involved in *Bordetella* infection–induced IL-10 production, DC2.4 cells were treated with leptomycin B, an inhibitor of nuclear export, and then infected with WT or ΔBopN (Fig. 8 F). The enhanced production of IL-10 in DC2.4 cells infected with WT *Bordetella* was significantly reduced in the presence of leptomycin B. Immunofluorescence microscopy analyses showed that NF-κBp65 could be detected in the nuclei of DC2.4 cells infected with WT *Bordetella* in the presence of leptomycin B (unpublished data). Conversely, the amounts of nuclear NF-κBp50 in DC2.4 cells infected with WT *Bordetella* were somewhat reduced in the presence of leptomycin B. In contrast to WT infection, localization of neither NF-κB p65 nor p50 in DC2.4 cells infected with ΔBopN was affected by leptomycin B (unpublished data). Thus, altered NF-κB translocation may contribute to the effects of BopN on the up-regulation of IL-10.

BopN alone modulates nuclear NF-κB subunit compartmentalization and down-regulates MAPK signaling

To analyze the precise function of BopN in the process of NF-κB nuclear translocation, we constructed expression vectors for the production of BopN fused with a Myc-tag, BopN

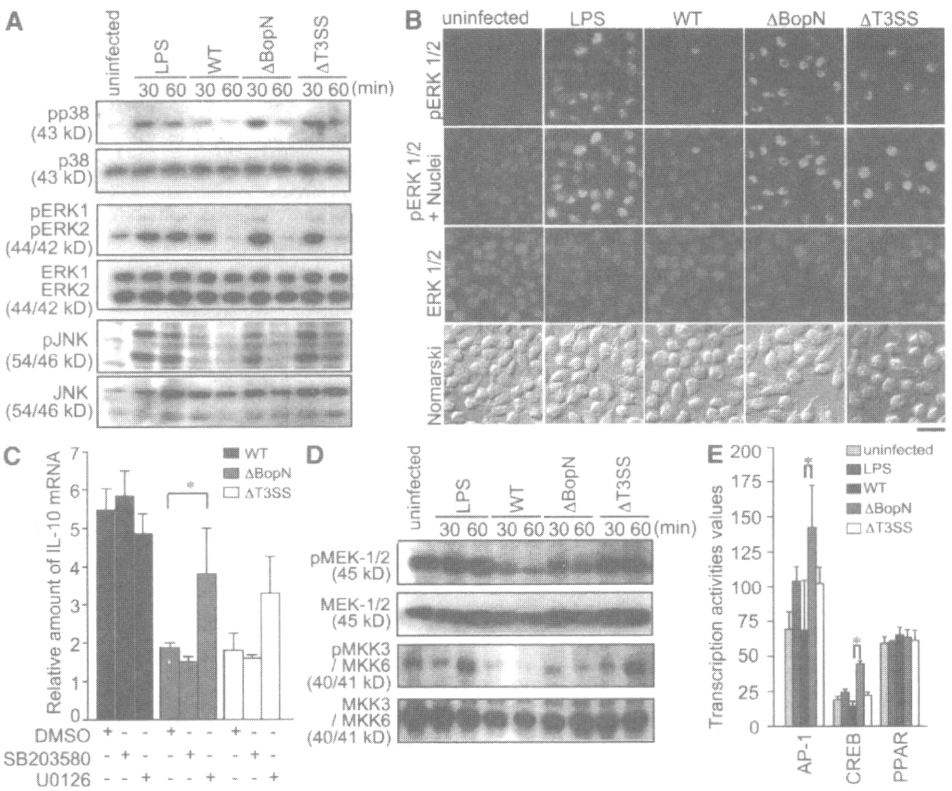

Figure 7. Molecular characterization of the function of BopN in MAPK pathways. (A) Immunoblot analysis of MAPK activities in the lysates of DC2.4 cells. DC2.4 cells were stimulated with 10 μg/ml LPS or infected with the indicated *Bordetella* strains for the specified time periods. The lysates were analyzed by Western blotting with antibodies against phospho-p38 (top), phospho-ERK1/2 (third from top), and phospho-JNK (fifth from top). The membranes were stripped and reblotted with antibodies against p38 (second panel), ERK1/2 (fourth from top), and JNK (bottom). (B) Immunofluorescence microscopy of DC2.4 cells stimulated with LPS for 30 min or infected for 30 min with the indicated strains. DC2.4 cells were fixed and stained with anti–phospho-ERK1/2 (green), anti-ERK1/2 (red), and DAPI (blue). Data are representative of three independent experiments. Bar, 20 μm. (C) 10 μM of MEK1/2 inhibitor U0126, 50 μM of p38 kinase inhibitor SB203580, and vehicle control (DMSO) were added to DC2.4 culture medium for 1 h before infection (m.o.i. = 100) with the indicated strains. Total RNA was prepared from the treated cells, and the amounts of IL-10 mRNA produced were assessed by qRT-PCR. (D) DC2.4 cells were infected with the indicated strains (m.o.i. = 100) for the specified time periods, and the amounts of phospho-MEK1/2 and phospho-MKK3/MKK6 were analyzed using immunoblotting. Three independent experiments were performed and a representative immunoblot is shown. (E) DC2.4 cells were stimulated with 10 μg/ml LPS or infected with the indicated strains for 30 min, and nuclear fractions were prepared and analyzed using a Multiplex transcription factor profiling kit. Differences in transcription factor activation were determined by Bio-Plex. The values in C and E are means ± SE from three independent experiments. *, $P < 0.05$.

full length (pBopN-FL; aa 1–365), BopN N-terminal half (pBopN-NT; aa 1–182), and BopN C-terminal half (pBopN-CT; aa 182–365), and the resulting constructs were introduced into Cos7 cells (Fig. 9, A–C). Interestingly, the N-terminal half (aa 1–182) of BopN was sufficient for the translocation of BopN into the nucleus, although the C-terminal half was required to completely block NF-κBp65 nuclear translocation. In contrast to NF-κBp65, most of the NF-κBp50 was localized in the cytosol of control Cos7 cells (vector alone), but translocation of NF-κBp50 into nuclei was facilitated by introduction of pBopN-FL (Fig. 9, A–C). Similar observations were obtained upon introduction of pBopN-FL into a macrophage cell line, RAW264.7, and nuclear translocation of BopN was detected in the presence

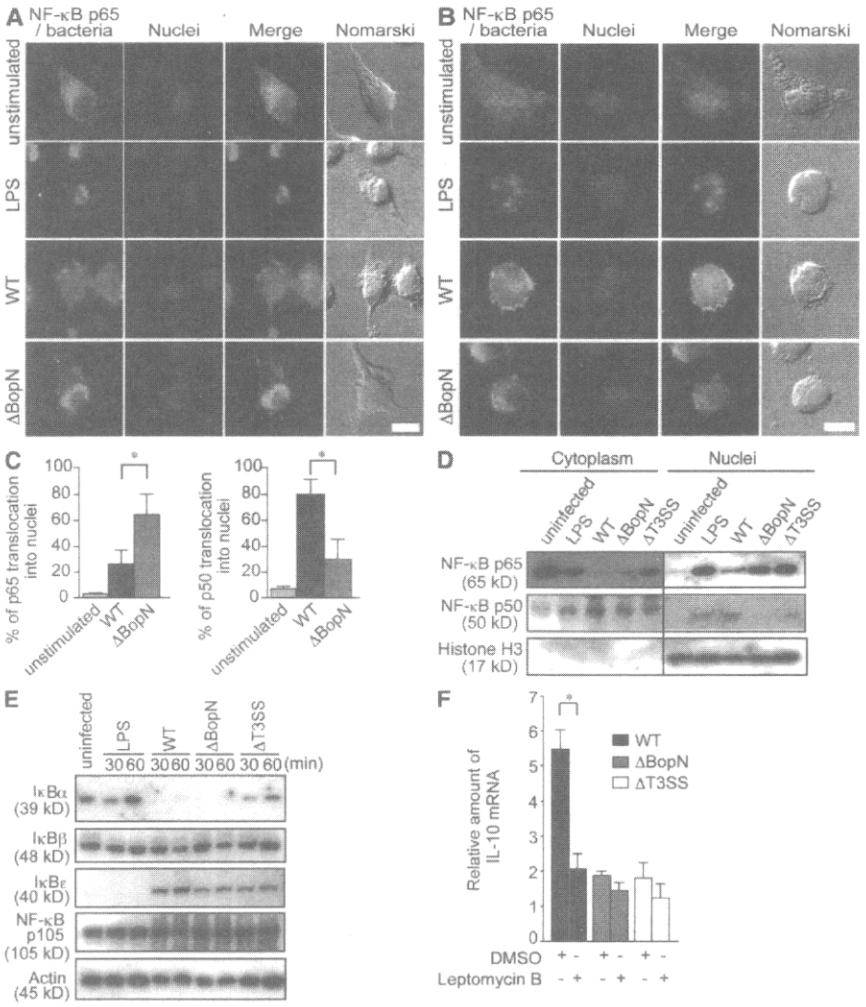

Figure 8. Molecular characterization of the mechanism by which BopN affects NF-κB pathways. (A and B) Immunofluorescence microscopy of DC2.4 cells 30 min after stimulation with 10 μg/ml LPS or infection with WT or ΔBopN *Bordetella* (m.o.i. = 100). The cells were stained with anti-*B. bronchiseptica* antibodies (red), anti-NF-κBp65 (A, green), or NF-κBp50 (B, green) antibodies, and DAPI for nuclei (blue). Bars, 10 μm. (C) DC2.4 cells infected with WT or ΔBopN *Bordetella* were randomly picked from the immunofluorescence micrographs (A and B), and the percentages of cells showing nuclear translocation of NF-κBp65 (left) or NF-κBp50 (right) were determined. Percentages were based on a count of 50 cells, and the values are means ± SD from three independent experiments. *, $P < 0.05$. (D) DC2.4 cells were stimulated by 10 μg/ml LPS or infected with the indicated strains for 30 min, and then separated into nuclear and cytosolic fractions. The resulting fractions were subjected to immunoblot analyses using anti-NF-κBp65 and anti-NF-κBp50 antibodies. Histone H3 antibodies were used as a nuclear control. The majority of both p65 and p50 was localized in the cytoplasm (A, B, and D) of unstimulated cells. (E) Immunoblot analysis of IκBα, IκBβ, IκBε, or NF-κBp105 in the lysates of DC2.4 cells. DC2.4 cells were stimulated with 10 μg/ml LPS or infected with the indicated strains, and total cell lysates were analyzed using immunoblotting with anti-IκBα, anti-IκBβ, anti-IκBε, or anti-NF-κBp105 antibodies. (F) 20 nM leptomycin B, an inhibitor of nuclear export, or vehicle control (DMSO) was added to DC2.4 culture medium for 24 h before infection with the indicated strains. Total RNA was prepared from DC2.4 cells, and amounts of IL-10 mRNA were assessed by qRT-PCR. The values are means ± SE from three independent experiments. *, $P < 0.05$.

or absence of LPS (Fig. S3). Collectively, our results show that BopN has the ability to translocate itself into the nucleus and promotes nuclear translocation of NF-κBp50.

To further investigate whether BopN is directly involved in the down-regulation of MAPK signaling, pBopN-FL was introduced into RAW264.7 cells and MAPK activity was analyzed by immunoblotting (Fig. 9 D). The amounts of phospho-ERK2 and phospho-p38 in RAW264.7 were increased by LPS stimulation. However, the activation (phosphorylation) of both MAPKs was reduced by the introduction of pBopN-FL into RAW264.7 cells. Interestingly, the level of IL-10 mRNA was significantly increased by introduction of pBopN-FL into RAW264.7 cells (Fig. 9 E). These results clearly indicate that BopN alone has an ability to induce IL-10 production by down-regulation of the MAPK signaling pathways. To eliminate the possibility that the enhanced production of IL-10 down-regulates MAPKs, IL-$10^{-/-}$–BMDCs were infected with WT or ΔBopN *Bordetella* and alterations in MAPKs were detected with immunoblotting (Fig. S4). During *Bordetella* infection, the levels of active or inactive

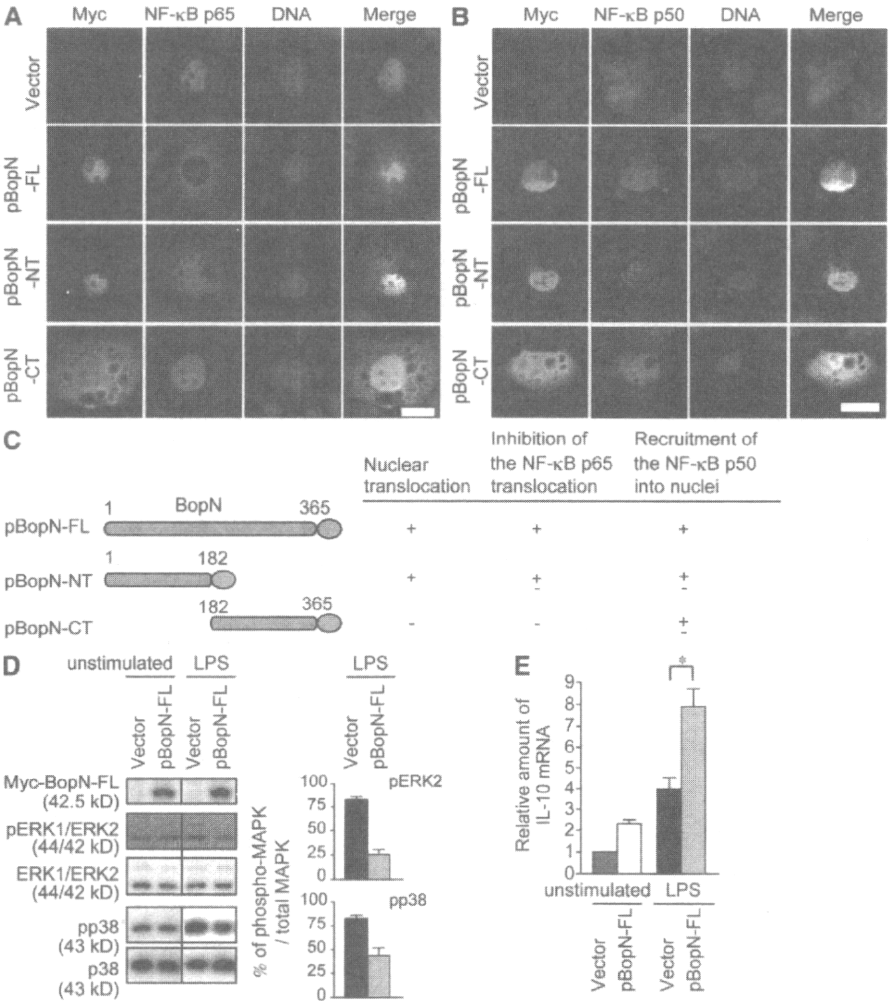

Figure 9. BopN alters the nuclear compartmentalization of NF-κB. (A and B) A mammalian expression vector, pcDNA3.1/His(-)A, encoding the full-length BopN-FL (aa 1–365) or truncated versions of BopN (-NT, aa 1–182; -CT, aa 182–365) with a Myc-tag fused at its C terminus was introduced into Cos7 cells. 24 h after transfection, cells were stimulated with 10 μg/ml LPS for 10 min, and then fixed and stained with anti-Myc antibodies to detect BopN (green), anti-NF-κBp65 (A, red), or NF-κBp50 (B, red), and DAPI for nuclei (blue). Bars, 20 μm. (C) Schematic diagrams of BopN fusion constructs with a Myc-tag (green) used in translocation assays (A and B). aa numbers of full-length and truncated BopN are shown. (D) The pBopN-FL was introduced into RAW264.7 cells. After LPS stimulation for 30 min, BopN-Myc fusion protein and phospho-MAPKs were detected by immunoblot analysis (left). Band intensity of phospho-ERK2 and phospho-p38 were quantified by the ImageJ application (right). The percentages of phospho-MAPK/total MAPK were determined from three independent experiments. (E) The level of IL-10 mRNA in RAW264.7 cells transfected with pBopN-FL was measured by qRT-PCR. The values presented for D and E are means ± SE from three independent experiments. *, $P < 0.05$.

MAPKs in IL-10$^{-/-}$–BMDCs were similar to those in WT-BMDCs, and the down-regulation of MAPK signaling by BopN also occurred in the absence of IL-10. These results suggest that altered MAPK activation can be attributed to BopN function and not to the enhanced production of IL-10.

DISCUSSION

BopN has long been thought to be a regulator for the *Bordetella* T3SS, because BopN shows weak homology (19%) to *Yersinia* YopN, which functions as a regulator to block secretion of Yop effectors (Forsberg et al., 1991). Secretion of Yop effectors via the T3SS is induced by contact between the bacterium and the host cell. In vitro, Yop secretion is dependent on calcium, being blocked in the presence and induced in the absence of calcium (Michiels et al., 1990). The block of Yop secretion in the presence of calcium requires a functional YopN; YopN deficiency results in constitutive secretion of Yop proteins in the presence or absence of calcium and before contact with the host cell (Forsberg et al., 1991). In this study, we demonstrated that BopN is an effector protein but not a regulator of other Bop proteins, and that the BopN effector translocates itself into the nuclei of host cells and triggers the up-regulation of IL-10. This alters the microenvironment and allows *Bordatella* to escape from the host immune system. We also have confirmed that the *Bordetella* BopN-deficient strain does not affect secretion of other type III–secreted proteins during in vitro growth (unpublished data).

In *B. bronchiseptica*, the gene encoding BopN is located within the Bsc T3SS locus, and BopN in *B. bronchiseptica* shows extensive identity (99%) to the BopN of *B. pertussis* Tohama I and *B. parapertussis* 12822, suggesting that the function of BopN is probably equivalent throughout the *Bordetella* species. To our knowledge, two effectors, BopC and BopN (this study), have been identified and characterized in *B. bronchiseptica*. The BopC effector induces necrotic cell death in infected cultured cells (Panina et al., 2005; Kuwae et al., 2006). However, as shown in Fig. 3 A, no histopathological lesions, including disruption of ciliated cells, were detected in mice infected with WT *B. bronchiseptica* (BopC-positive phenotype), suggesting that the respiratory tract is not a BopC target.

To evade the host immune system, certain bacterial pathogens have evolved strategies to subvert activation of host signaling pathways. For example, *Shigella* delivers OspF into the host cell via T3SS. This effector is translocated into the nucleus and dephosphorylates MAPKs, thereby preventing phosphorylation of histone H3 at Ser10 (Arbibe et al., 2007). Thus, epigenetic modification by the OspF effector results in inhibition of NF-κB chromatin access leading to the inactivation of IL-8 and other genes essential for innate immune responses (Thomson et al., 1999; Saccani et al., 2002; Arbibe et al., 2007). Recently, OspF was characterized as a phosphothreonine lyase, which removes phosphate groups from the phosphothreonine residues of MAPKs (Li et al., 2007). However, BopN has no sequence similarity to OspF and does not contain His-Cys-X5-Arg-Ser/Thr, a catalytic active site for specific phosphatases (Zhang, 2002). The precise mechanism by which MAPK is inactivated is unclear, but this signaling pathway is a target of BopN function (Fig. 7 and Fig. 9).

We have shown that *Bordatella* evades the host immune system and establishes persistent colonization via induction of IL-10. In general, ERK activation is required for host cells to produce high IL-10. However, our results clearly indicate that blockade of the ERK pathway by the specific MEK inhibitor U0126 allowed enhanced production of IL-10 in DC2.4 cells infected with ΔBopN (Fig. 7 C). In contrast, pharmacological blockade of p38 activation does not affect IL-10 induction. Although the functional significance of altered JNK activation is still unclear, these results suggest that BopN regulation of IL-10 is mediated, at least in part, by its ability to modulate ERK activation.

The transcription factor NF-κB, which consists of homo- and heterodimers of the p50, p52, p65 (also called RelA), RelB, and c-Rel subunits, plays a central role in regulating host immune and inflammatory responses (Baldwin, 1996; Ghosh et al., 1998; Karin and Ben-Neriah, 2000). In unstimulated cells, NF-κB is associated with members of the IκB protein family in the cytoplasm as an inactive form. When a bacterial pathogen enters the host, various stimuli are detected by Toll-like receptors (TLRs) and nucleotide-binding oligomerization domain protein–like receptors. These signaling pathways trigger activation of the IκB kinase to phosphorylate IκBs, leading to ubiquitination of phospho-IκBs and their degradation via the ubiquitin–proteasome pathway, thus permitting nuclear translocation of NF-κB. (Sun and Ley, 2008). Nuclear NF-κB activates the expression of immunoregulatory genes, including IFN-γ, as well as several other proinflammatory cytokines. Expression of these genes is required for the triggering of inflammatory responses that eliminate bacterial pathogens by innate immunity. The subversion of the NF-κB signaling pathway is a bacterial mechanism by which to evade the host immune system. For example, *Shigella* OspG effector associates with ubiquitin-conjugating enzymes that ubiquitinate phospho-IκBα, thus blocking NF-κB translocation into nuclei (Kim et al., 2005). We showed that IκBα degradation is not affected by BopN function (Fig. 8 E). Furthermore, although OspG must be located in the host cytosol to exert its effects on degradation of phospho-IκBα, our data clearly showed that the BopN effector has the ability to independently translocate itself into the nucleus and contains a nuclear localization signal located in the N-terminal half (aa 1–182; Fig. 9). It has been reported that *Bordetella* inhibits the nuclear translocation of NF-κBp65 in a T3SS-dependent manner (Yuk et al., 2000). In this study, we showed that BopN blocks nuclear translocation of NF-κBp65 and promotes nuclear translocation of NF-κBp50. The translocation of NF-κBp50 into the nucleus is involved in the up-regulation of IL-10, as previously described (Driessler et al., 2004; Cao et al., 2006). As shown in Fig. 8 F, leptomycin B inhibits IL-10 production, suggesting that the relocation of NF-κB components contributes to the effects of BopN on IL-10 production.

In *Yersinia*, LcrV is located at the tip of the T3SS needle structure (Mueller et al., 2005) and is involved in effector translocation. LcrV reportedly enhances production of IL-10 via association with TLR2 (Sing et al., 2005). However, $TLR2^{-/-}$ mice were not protected against subcutaneous plague infection (Pouliot et al., 2007). Recently, Depaolo et al. (2008) demonstrated that LcrV-mediated TLR6 is involved in the up-regulation of IL-10 via activation of the JNK pathway. They further confirmed that IL-$10^{-/-}$ and $TLR6^{-/-}$ mice are significantly protected from plague infection. Thus, both *Bordetella* and *Yersinia* species induce the up-regulation of IL-10, but they exploit different host-cell signaling pathways using different virulence factors.

We demonstrated that BopN has the ability to alter both MAPKs and the nuclear translocation of NF-κB, resulting in activation or inactivation of various transcriptional factors. Furthermore, we confirmed that NF-κB activation in DC2.4 cells infected with ΔBopN was similar to that of DC2.4 cells infected with WT (Fig. S5). To our surprise, the level of CRE-ATF, Myc-Max, and SP-1 activation in DC2.4 cells was significantly increased after infection with WT relative to ΔBopN, even though, in general, activation of these transcription factors is dependent on MAPK signaling. SP-1 plays an important role in IL-10 transcription (Chanteux et al., 2007). Thus, *Bordetella* appears to exploit a transcription factor, SP-1, for the up-regulation of IL-10 during infection, although the BopN-mediated signaling pathway remains to be fully elucidated.

Phagocytosed *B. pertussis* bacteria are easily killed by neutrophils (Lenz et al., 2000) and IFN-γ production is required for *Bordetella* clearance from the lung (Pilione and Harvill, 2006). Our in vivo successive infection study directly showed that IFN-γ production is involved in *Bordetella* clearance and that mice can survive a lethal dose of WT *Bordetella* when the up-regulation of IL-10, as a *Bordetella* strategy, was perturbed by preinfection with the avirulent ΔBopN strain (Fig. 6). Recently, it was reported that the T3SS of *B. pertussis* is also involved in persistent colonization in mice and that, indeed, BopN was detected as a protein secreted via T3SS (Fennelly et al., 2008). Another study showed that *B. pertussis* can induce IL-10 production in BMDCs (McGuirk et al., 2002). Thus, the up-regulation of IL-10 by the BopN effector is likely a stealth strategy by which *Bordetella* establishes an immunosuppressive environment such that the resulting microenvironment is advantageous for persistent colonization.

MATERIALS AND METHODS

Bacterial strains and plasmids. *E. coli* DH10B, MC1061, and SM10λ*pir* were used as hosts for the construction of various plasmids. The WT strain used in this study was *B. bronchiseptica* S798 (Kuwae et al., 2003). The type III secretion mutant (ΔT3SS) and BopC mutant (ΔBopC) were derived from S798 WT (Kuwae et al., 2003, 2006). The inoculum for liquid culture of *Bordetella* strains was prepared from fresh colonies grown on Bordet-Gengou (BG) agar, and these bacteria were cultured in Stainer-Scholte liquid medium at a starting A_{600} of 0.2 with vigorous shaking at 37°C for 18 h, as previously described (Cotter and Miller, 1994, 1997; Martínez de Tejada et al., 1996). The *B. bronchiseptica* strain BopN mutant (ΔBopN) was created as follows. pDONR201 (Invitrogen) and pABB-CRS2 (Sekiya et al., 2001) were used as the cloning and positive suicide vectors, respectively. A 2.4-kbp DNA fragment containing the *bopN* gene was amplified by PCR with the primers B1-*bopN* (5′-AAAAAGCAGGCTCC-GCCTGGGCCTCGGCCTCT-3′) and B2-*bopN* (5′-AGAAAGCTGGGT-GCCAGGGCCAGCAGGGACC-3′) using *B. bronchiseptica* S798 genomic DNA as the template. The resulting PCR product was cloned into pDONR201 to obtain pDONR-*bopN* using the adaptor PCR method in the Gateway cloning system (Invitrogen). Inverse PCR was performed with the primers R1-*bopN* (5′-GGAATTCATTGGGGGCGGCATCGATAC-3′) and R2-*bopN* (5′-GGAATTCAACGCGATAGCAATGGAGAA-3′) using circular pDONR-*bopN* as the template. The underlined portions indicate the EcoRI sites. The resulting PCR products were digested with EcoRI and self-ligated to obtain pDONR-Δ*bopN*, which contained a 1,044-bp deletion within the open reading frame of *bopN*. pDONR-Δ*bopN* was mixed with pABB-CRS2 to obtain pABB-Δ*bopN* using the Gateway cloning system. pABB-Δ*bopN* was introduced into *E. coli* SM10λ*pir* and was transconjugated into the *B. bronchiseptica* S798 (streptomycin resistant), as previously described (Donnenberg and Kaper, 1991). The resulting mutant strain was designated as *B. bronchiseptica* ΔBopN. For the complementation of the *bopN* defect in ΔBopN, pBopN was constructed as follows. A 1.2-kbp fragment encoding *bopN* was amplified by PCR with the primers B1-*bopN*–comp (5′-AAAAAGCAGGCTGCGACACTCACTGCACCAGT-3′) and B2-*bopN*–comp (5′-AGAAAGCTGGGTATCCTGGCCGAACTGATGCA-3′) using *B. bronchiseptica* S798 genomic DNA as the template. The resulting fragment was cloned into pDONR201 and designated as pDONR-*bopN*–comp. To control the transcription of the *bopN* gene by the *fha* promoter and *rrnB* terminator in *Bordetella*, pDONR-*fhaP* (Kuwae et al., 2006), pDONR-*bopN*–comp, pDONR-*rrnB* (Kuwae et al., 2006), and pRK415 R4-R3-F (Kuwae et al., 2006) were mixed and treated with LR Clonase Plus (Invitrogen) to clone the *fha* promoter, *bopN*, and *rrnB* terminator into pRK415 R4-R3-F using the MultiSite Gateway system (Invitrogen), and the resulting plasmid was designated as pBopN. To express the BopN-Myc fusion protein in mammalian cells, pBopN-FL was constructed as follows. The *bopN* gene was amplified by PCR with the primers 5′-GGAATTCGCCAC-CATGGCTCGTATCGATGCCG-3′ (forward) and 5′-CGGGATCCT-GCGTTCTCCATTGCTATCG-3′ (reverse) using *B. bronchiseptica* S798 genomic DNA as the template. To obtain the plasmid encoding truncated versions of the BopN-NT or BopN-CT, PCR was performed with the primer sets 5′-GGAATTCGCCACCATGGCTCGTATCGATGCCG-3′ (forward) and 5′-CGGGATCCCGCTTGCGCGGCCAGTTGC-3′ (reverse) or 5′-GGAATTCGCCACCATGGGTGTCACGCAGCAATACC-3′ (forward) and 5′-CGGGATCCTGCGTTCTCCATTGCTATCG-3′ (reverse). The underlined portions, GAATTC and GGATCC, indicate the EcoRI and BamHI sites, respectively. The EcoRI-BamHI fragment of the resulting PCR product was cloned into the EcoRI and BamHI sites of pcDNA3.1/His(-)A (Invitrogen) to obtain pBopN-FL, pBopN-NT, and pBopN-CT, respectively.

Mice. 5–6-wk-old C57BL/6J mice were purchased from Nihon SLC. IL-$10^{-/-}$ mice on a C57BL/6J background were obtained from the Jackson Laboratory.

Cells and transfection. The DC line DC2.4 was provided by K.M. Rock (University of Massachusetts, Worcester, MA) and grown in RPMI 1640 (Invitrogen) containing 10% FCS (Sigma-Aldrich), 55 μM 2-mercaptoethanol, 100 U/ml penicillin, and 100 μg/ml streptomycin at 37°C under an atmosphere of 5% CO_2. Cos7 cells (American Type Culture Collection) were maintained in Dulbecco's modified Eagle's medium (Sigma-Aldrich) with 10% FCS. The mouse macrophage cell line RAW264.7 (American Type Culture Collection) was maintained in RPMI 1640 medium with 10% FCS. Cos7 and RAW264.7 cells were transfected with 2.5 μg/ml pcDNA3.1/His(-)A, pBopN-FL, pBopN-NT, and pBopN-CT using Lipofectamine LTX (Invitrogen) according to the manufacturer's protocol. After transfection, the cells were incubated at 37°C for 24 h and fixed in 4% paraformaldehyde.

Inhibitors. For the MAPK inhibition experiments, the MEK1/2 inhibitor U0126 (EMD) or the p38 kinase inhibitor SB203580 (EMD) was added to medium at 10 and 50 μM, respectively, for 1 h before LPS stimulation or *Bordetella* infection. To block nuclear export, leptomycin B (EMD) was added to medium at 20 nM for 24 h before the *Bordetella* infection.

Preparation of DCs from BM. BM cells prepared from the tibias and femurs of mice were cultured at 1.5×10^6 cells/ml in RPMI 1640 medium with 10% FCS in the presence of 10 ng/ml GM-CSF (Fitzgerald Industries). BM cells were maintained for 3 d, and then one half of the medium was replaced by fresh medium. BM cells were further maintained for 3 d, and then DCs were purified using anti-CD11c microbeads with an autoMACS separation system (Miltenyi Biotec) .

LDH assay. DC2.4 cells were seeded in 24-well plates at 2.5×10^5 cells/well and incubated for 20 h. The precultured bacteria described in Bacterial strains and plasmids were added to the cells at a multiplicity of infection (m.o.i.) of 10 and centrifuged for 5 min. After incubation at 37°C under an atmosphere of 5% CO_2 for the time periods indicated in the figures, the amounts of LDH were measured spectrophotometrically using a CytoTox 96 Non-Radioactive Cytotoxicity Assay kit (Promega).

In vivo infection of mice. After arrival, all mice were housed for 1 wk before experiments. Mice were infected intranasally with 50 μl (5×10^6 or 5×10^5 CFU) of a *B. bronchiseptica* overnight culture started from an individually isolated colony on BG agar plates. To determine the amount of bacterial colonization in the lung, the whole lung was homogenized in 10 ml of cold PBS using a digital homogenizer (Potter-Elvehjem; As One, Inc.). The resulting homogenates were serially diluted with cold PBS and plated on BG agar plates, and colonies were then counted to calculate the number of CFUs per mouse. For histological analysis, lung tissues were fixed in 4% paraformaldehyde in PBS and stained with H&E. For detection of DCs or macrophages that had migrated into the lung, lung tissues were fixed and immunostained with anti-CD11c monoclonal antibodies (Endogen). For scanning electron microscopy observation, trachea sections were fixed in 2.5% glutaraldehyde in PBS. Three 5–6-wk-old mice were used for each time point. All animal experiments were conducted according to protocols approved by the Experimental Animal Center of the Kitasato University.

Flow cytometry. Lung cells were incubated in 100 μl DMEM at 4°C for 1 h and stained with PE-Cy7–conjugated anti–Gr-1 (clone RB6-8c5; eBioscience), FITC-conjugated anti-CD11b (clone M1/70; BD), and PE-conjugated anti-CD11c (clone HL3; BD). For ex vivo intracellular cytokine staining, lung cells were cultured at 37°C for 4.5 h in PBS supplemented with 2% FCS and GolgiStop (BD). Cells were stained with PE-conjugated anti-CD11c antibodies, and then fixed and permeabilized with Cytofix/Cytoperm solution (BD). After fixation and permeabilization, cells were stained with FITC-conjugated anti–IL-10 (clone JES5-16E3; BD). Flow cytometric analysis (FACS) was performed with a multi–flow cytometry system (EPICS Elite; Beckman Coulter) using the EXPO 32 Elite software package (Beckman Coulter).

Fluorescence staining. DC2.4 cells were seeded in a 6-well plate at 5×10^5 cells/well and incubated for 20 h, and then infected with *Bordetella* strains at an m.o.i. of 10. After 60 min, DCs were fixed for 15 min with 4% paraformaldehyde in PBS and subjected to immunofluorescence staining with anti–NF-κBp65 and anti–NF-κBp50 antibodies (Santa Cruz Biotechnology, Inc.). As a secondary antibody, Alexa Fluor 488 goat anti–rabbit IgG (Invitrogen) was used. Nuclei were stained with DAPI (Invitrogen). Bacteria were visualized with rabbit anti–*B. bronchiseptica* serum (Denka Seiken) followed by Alexa Fluor 594–conjugated secondary antibody. Numbers of NF-κBp65 translocated into nuclei were scored by examining 50 cells per coverslip under a fluorescence microscope. Phosphorylated or total ERKs were stained with anti–phospho-ERK or anti-ERK antibody (Cell Signaling Technology), and Alexa Fluor 488 goat anti–mouse IgG or Alexa Fluor 594 goat anti–rabbit IgG (Invitrogen) were used as secondary antibodies, respectively. BopN-Myc fusion proteins were stained with anti-Myc antibody (Santa Cruz Biotechnology, Inc.) and Alexa Fluor 488 goat anti–mouse IgG (Invitrogen).

mRNA analysis by real-time PCR. DC2.4 cells were seeded in 24-well plates at 2.5×10^5 cells/well, incubated for 20 h, and infected with *Bordetella* strains at an m.o.i. of 10. After incubation for the times indicated in the figures, total RNA was isolated using an RNeasy Mini Kit (QIAGEN), and 5 μg RNA from each sample was reverse transcribed using oligo (dT) primers and Omniscript RT (QIAGEN). The resulting 5 μl cDNA was amplified by SYBR Premix Ex Taq (Takara Bio Inc.) using mouse IL-10 primers and β-actin primers in a LightCycler apparatus (Roche). Primer pairs specific for IL-10 (forward, 5′-AGCTGGACAACATACTGCTA-3′; reverse, 5′-TGGGCCATGCTTCTCTG-3′) and β-actin (forward, 5′-GTGGGCCGCTCTAGCCACCAA-3′; reverse, 5′-TCTTTGATGTCACGCACGATTTC-3′) were used. The specificity was checked by analyzing the melting curves, and results were calculated using the comparative cycle threshold method, in which the amount of target mRNA is normalized to the internal control β-actin and calculated in arbitrary units set to a value of 1 for uninfected cells.

Cytokine detection. Lung specimens were homogenized as described in In vivo infection of mice, and concentrations of IL-10 or IFN-γ in the homogenates were determined by an ELISA development kit (DuoSet; R&D Systems). The absorbance of each well was determined using a plate reader (Biotrak II; GE Healthcare).

Immunoblotting. DC2.4 cells infected with *B. bronchiseptica* were washed with PBS and solubilized with SDS sample buffer. The resulting samples were sonicated and boiled for 5 min, separated by SDS-PAGE on a 10% gel, and transferred to polyvinylidene fluoride membranes (Millipore). Proteins were analyzed by immunoblotting with anti–phospho–p38 MAPK (Thr180/Tyr182), anti–phospho–p44/p42 MAPK (Thr202/Tyr204; E10), anti–phospho–stress-activated protein kinase (SAPK)/JNK (Thr183/Tyr185), anti–phospho-MEK1/2 (Ser217/221), and anti–phospho-MKK3/MKK6 (Ser189/207) antibodies (Cell Signaling Technology). Anti-IκBα, anti-IκBβ, anti-IκBε, and anti–NF-κBp105 antibodies (Cell Signaling Technology) were used to detect IκBα, IκBβ, IκBε, and NF-κBp105, respectively. To ensure equal protein loading, the membrane was stripped and reprobed with anti–p38 MAPK (Santa Cruz Biotechnology, Inc.), anti–p44/p42 MAPK, anti-SAPK/JNK, anti-MKK3, anti-MEK1/2 (47E6), or anti–β-actin antibodies (Cell Signaling Technology). The detection of specific protein signals was performed using a detection kit (ECL; GE Healthcare). Nuclear and cytosolic fractions were prepared using a subcellular proteome extraction kit (ProteoExtract; EMD). Lysates of DC2.4 cells infected with *B. bronchiseptica* were separated into nuclear and cytosolic fractions, and the resulting fractions were analyzed by immunoblotting with anti–NF-κBp65 and anti–NF-κBp50 (Santa Cruz Biotechnology, Inc.), and anti–histone H3 (Cell Signaling Technology) antibodies. Protein expression levels were determined by densitometry analysis of immunoblots using ImageJ (version 1.42; National Institutes of Health).

Transcription factor profiling. Nuclear fractions were prepared from DC2.4 cells infected with *B. bronchiseptica* using the ProteoExtract subcellular proteome extraction kit and analyzed using a transcription factor profiling kit (Multiplex; Marligen). Positive binding of each transcription factor to the DNA probe was detected using Bio-Plex (Bio-Rad Laboratories).

Statistics. Statistical analyses were performed using the Mann-Whitney *U* test or the unpaired Student's *t* test, with $P < 0.05$ considered statistically significant. Survival curves were generated by the Kaplan-Meier method, and statistical analyses were performed using the log-rank test.

Online supplemental material. Fig. S1 shows H&E staining of lung sections of mice infected with *B. bronchiseptica*. Fig. S2 shows densitometry analyses of immunoblots, immunofluorescence micrographs of MAPK

activities, and confirmation of the specificity of anti-ERK antibodies by immunoblotting. Fig. S3 shows immunofluorescence micrographs to identify localization of NF-κBp65 and NF-κBp50 in a macrophage cell line transfected with a *bopN* clone. Fig. S4 shows immunoblot analysis of phospho-MAPKs in WT- and IL-$10^{-/-}$–derived BMDCs infected with *B. bronchiseptica*. Fig. S5 shows transcription factor profiling during the *Bordetella* infection. Online supplemental material is available at http://www.jem.org/cgi/content/full/jem.20090494/DC1.

Dr. C. Sasakawa has generously reviewed the paper and gave us critical comments.

This work was supported in part by the Ministry of Education, Culture, Sports, Science, and Technology of Japan through Grants-in-Aid for Scientific Research (B, 18390136 and 21390133) and for Scientific Research on Priority Areas (19041066 and 21022045). Support was also received in the form of operating grants from a Kitasato University Research Grant for Young Researchers (2008).

S. Koyasu is a consultant for Medical and Biological Laboratories, Co. Ltd. The authors otherwise have no financial conflicts of interest.

Submitted: 4 March 2009
Accepted: 13 November 2009

REFERENCES

Abe, A., U. Heczko, R.G. Hegele, and B. Brett Finlay. 1998. Two enteropathogenic *Escherichia coli* type III secreted proteins, EspA and EspB, are virulence factors. *J. Exp. Med.* 188:1907–1916. doi:10.1084/jem.188.10.1907

Arbibe, L., D.W. Kim, E. Batsche, T. Pedron, B. Mateescu, C. Muchardt, C. Parsot, and P.J. Sansonetti. 2007. An injected bacterial effector targets chromatin access for transcription factor NF-kappaB to alter transcription of host genes involved in immune responses. *Nat. Immunol.* 8:47–56. doi:10.1038/ni1423

Baldwin, A.S., Jr. 1996. The NF-κB and IκB proteins: new discoveries and insights. *Annu. Rev. Immunol.* 14:649–683. doi:10.1146/annurev.immunol.14.1.649

Cao, S., X. Zhang, J.P. Edwards, and D.M. Mosser. 2006. NF-kappaB1 (p50) homodimers differentially regulate pro- and anti-inflammatory cytokines in macrophages. *J. Biol. Chem.* 281:26041–26050. doi:10.1074/jbc.M602222200

Chanteux, H., A.C. Guisset, C. Pilette, and Y. Sibille. 2007. LPS induces IL-10 production by human alveolar macrophages via MAPKinases- and Sp1-dependent mechanisms. *Respir. Res.* 8:71. doi:10.1186/1465-9921-8-71

Cotter, P.A., and J.F. Miller. 1994. BvgAS-mediated signal transduction: analysis of phase-locked regulatory mutants of *Bordetella bronchiseptica* in a rabbit model. *Infect. Immun.* 62:3381–3390.

Cotter, P.A., and J.F. Miller. 1997. A mutation in the *Bordetella bronchiseptica* bvgS gene results in reduced virulence and increased resistance to starvation, and identifies a new class of Bvg-regulated antigens. *Mol. Microbiol.* 24:671–685. doi:10.1046/j.1365-2958.1997.3821741.x

Depaolo, R.W., F. Tang, I. Kim, M. Han, N. Levin, N. Ciletti, A. Lin, D. Anderson, O. Schneewind, and B. Jabri. 2008. Toll-like receptor 6 drives differentiation of tolerogenic dendritic cells and contributes to LcrV-mediated plague pathogenesis. *Cell Host Microbe.* 4:350–361. doi:10.1016/j.chom.2008.09.004

Donnenberg, M.S., and J.B. Kaper. 1991. Construction of an eae deletion mutant of enteropathogenic *Escherichia coli* by using a positive-selection suicide vector. *Infect. Immun.* 59:4310–4317.

Driessler, F., K. Venstrom, R. Sabat, K. Asadullah, and A.J. Schottelius. 2004. Molecular mechanisms of interleukin-10-mediated inhibition of NF-kappaB activity: a role for p50. *Clin. Exp. Immunol.* 135:64–73. doi:10.1111/j.1365-2249.2004.02342.x

Fauconnier, A., A. Veithen, P. Gueirard, R. Antoine, L. Wacheul, C. Locht, A. Bollen, and E. Godfroid. 2001. Characterization of the type III secretion locus of *Bordetella pertussis*. *Int. J. Med. Microbiol.* 290:693–705.

Fennelly, N.K., F. Sisti, S.C. Higgins, P.J. Ross, H. van der Heide, F.R. Mooi, A. Boyd, and K.H. Mills. 2008. *Bordetella pertussis* expresses a functional type III secretion system that subverts protective innate and adaptive immune responses. *Infect. Immun.* 76:1257–1266. doi:10.1128/IAI.00836-07

Finlay, B.B., and P. Cossart. 1997. Exploitation of mammalian host cell functions by bacterial pathogens. *Science.* 276:718–725. doi:10.1126/science.276.5313.718

Foley, J.E., C. Rand, M.J. Bannasch, C.R. Norris, and J. Milan. 2002. Molecular epidemiology of feline bordetellosis in two animal shelters in California, USA. *Prev. Vet. Med.* 54:141–156. doi:10.1016/S0167-5877(02)00022-3

Forsberg, A., A.M. Viitanen, M. Skurnik, and H. Wolf-Watz. 1991. The surface-located YopN protein is involved in calcium signal transduction in *Yersinia pseudotuberculosis*. *Mol. Microbiol.* 5:977–986. doi:10.1111/j.1365-2958.1991.tb00773.x

Galán, J.E., and H. Wolf-Watz. 2006. Protein delivery into eukaryotic cells by type III secretion machines. *Nature.* 444:567–573. doi:10.1038/nature05272

Ghosh, S., M.J. May, and E.B. Kopp. 1998. NF-κB and Rel proteins: evolutionarily conserved mediators of immune responses. *Annu. Rev. Immunol.* 16:225–260. doi:10.1146/annurev.immunol.16.1.225

Goodnow, R.A. 1980. Biology of *Bordetella bronchiseptica*. *Microbiol. Rev.* 44:722–738.

Gzyl, A., E. Augustynowicz, I. van Loo, and J. Slusarczyk. 2001. Temporal nucleotide changes in pertactin and pertussis toxin genes in *Bordetella pertussis* strains isolated from clinical cases in Poland. *Vaccine.* 20:299–303. doi:10.1016/S0264-410X(01)00356-5

He, Q., J. Mäkinen, G. Berbers, F.R. Mooi, M.K. Viljanen, H. Arvilommi, and J. Mertsola. 2003. *Bordetella pertussis* protein pertactin induces type-specific antibodies: one possible explanation for the emergence of antigenic variants? *J. Infect. Dis.* 187:1200–1205. doi:10.1086/368412

Karin, M., and Y. Ben-Neriah. 2000. Phosphorylation meets ubiquitination: the control of NF-[κ]B activity. *Annu. Rev. Immunol.* 18:621–663. doi:10.1146/annurev.immunol.18.1.621

Kim, D.W., G. Lenzen, A.L. Page, P. Legrain, P.J. Sansonetti, and C. Parsot. 2005. The *Shigella flexneri* effector OspG interferes with innate immune responses by targeting ubiquitin-conjugating enzymes. *Proc. Natl. Acad. Sci. USA.* 102:14046–14051. doi:10.1073/pnas.0504466102

King, A.J., G. Berbers, H.F. van Oirschot, P. Hoogerhout, K. Knipping, and F.R. Mooi. 2001. Role of the polymorphic region 1 of the *Bordetella pertussis* protein pertactin in immunity. *Microbiology.* 147:2885–2895.

Kuwae, A., M. Ohishi, M. Watanabe, M. Nagai, and A. Abe. 2003. BopB is a type III secreted protein in *Bordetella bronchiseptica* and is required for cytotoxicity against cultured mammalian cells. *Cell. Microbiol.* 5:973–983. doi:10.1046/j.1462-5822.2003.00341.x

Kuwae, A., T. Matsuzawa, N. Ishikawa, H. Abe, T. Nonaka, H. Fukuda, S. Imajoh-Ohmi, and A. Abe. 2006. BopC is a novel type III effector secreted by *Bordetella bronchiseptica* and has a critical role in type III-dependent necrotic cell death. *J. Biol. Chem.* 281:6589–6600. doi:10.1074/jbc.M512711200

Lenz, D.H., C.L. Weingart, and A.A. Weiss. 2000. Phagocytosed *Bordetella pertussis* fails to survive in human neutrophils. *Infect. Immun.* 68:956–959. doi:10.1128/IAI.68.2.956-959.2000

Li, H., H. Xu, Y. Zhou, J. Zhang, C. Long, S. Li, S. Chen, J.M. Zhou, and F. Shao. 2007. The phosphothreonine lyase activity of a bacterial type III effector family. *Science.* 315:1000–1003. doi:10.1126/science.1138960

Martínez de Tejada, G., J.F. Miller, and P.A. Cotter. 1996. Comparative analysis of the virulence control systems of *Bordetella pertussis* and *Bordetella bronchiseptica*. *Mol. Microbiol.* 22:895–908. doi:10.1046/j.1365-2958.1996.01538.x

Mattoo, S., and J.D. Cherry. 2005. Molecular pathogenesis, epidemiology, and clinical manifestations of respiratory infections due to *Bordetella pertussis* and other *Bordetella* subspecies. *Clin. Microbiol. Rev.* 18:326–382. doi:10.1128/CMR.18.2.326-382.2005

McGuirk, P., C. McCann, and K.H. Mills. 2002. Pathogen-specific T regulatory 1 cells induced in the respiratory tract by a bacterial molecule that stimulates interleukin 10 production by dendritic cells: a novel strategy for evasion of protective T helper type 1 responses by *Bordetella pertussis*. *J. Exp. Med.* 195:221–231. doi:10.1084/jem.20011288

Medhekar, B., R. Shrivastava, S. Mattoo, M. Gingery, and J.F. Miller. 2009. *Bordetella* Bsp22 forms a filamentous type III secretion system tip complex and is immunoprotective in vitro and in vivo. *Mol. Microbiol.* 71:492–504. doi:10.1111/j.1365-2958.2008.06543.x

Michiels, T., P. Wattiau, R. Brasseur, J.M. Ruysschaert, and G. Cornelis. 1990. Secretion of Yop proteins by Yersiniae. *Infect. Immun.* 58: 2840–2849.

Mueller, C.A., P. Broz, S.A. Müller, P. Ringler, F. Erne-Brand, I. Sorg, M. Kuhn, A. Engel, and G.R. Cornelis. 2005. The V-antigen of *Yersinia* forms a distinct structure at the tip of injectisome needles. *Science.* 310:674–676. doi:10.1126/science.1118476

Nogawa, H., A. Kuwae, T. Matsuzawa, and A. Abe. 2004. The type III secreted protein BopD in *Bordetella bronchiseptica* is complexed with BopB for pore formation on the host plasma membrane. *J. Bacteriol.* 186:3806–3813. doi:10.1128/JB.186.12.3806-3813.2004

Panina, E.M., S. Mattoo, N. Griffith, N.A. Kozak, M.H. Yuk, and J.F. Miller. 2005. A genome-wide screen identifies a *Bordetella* type III secretion effector and candidate effectors in other species. *Mol. Microbiol.* 58:267–279. doi:10.1111/j.1365-2958.2005.04823.x

Pilione, M.R., and E.T. Harvill. 2006. The *Bordetella bronchiseptica* type III secretion system inhibits gamma interferon production that is required for efficient antibody-mediated bacterial clearance. *Infect. Immun.* 74:1043–1049. doi:10.1128/IAI.74.2.1043-1049.2006

Pouliot, K., N. Pan, S. Wang, S. Lu, E. Lien, and J.D. Goguen. 2007. Evaluation of the role of LcrV-Toll-like receptor 2-mediated immunomodulation in the virulence of *Yersinia pestis*. *Infect. Immun.* 75:3571–3580. doi:10.1128/IAI.01644-06

Raguckas, S.E., H.L. VandenBussche, C. Jacobs, and M.E. Klepser. 2007. Pertussis resurgence: diagnosis, treatment, prevention, and beyond. *Pharmacotherapy.* 27:41–52. doi:10.1592/phco.27.1.41

Reissinger, A., J.A. Skinner, and M.H. Yuk. 2005. Downregulation of mitogen-activated protein kinases by the *Bordetella bronchiseptica* type III secretion system leads to attenuated nonclassical macrophage activation. *Infect. Immun.* 73:308–316. doi:10.1128/IAI.73.1.308-316.2005

Saccani, S., S. Pantano, and G. Natoli. 2002. p38-dependent marking of inflammatory genes for increased NF-κB recruitment. *Nat. Immunol.* 3:69–75. doi:10.1038/ni748

Sekiya, K., M. Ohishi, T. Ogino, K. Tamano, C. Sasakawa, and A. Abe. 2001. Supermolecular structure of the enteropathogenic *Escherichia coli* type III secretion system and its direct interaction with the EspA-sheath-like structure. *Proc. Natl. Acad. Sci. USA.* 98:11638–11643. doi:10.1073/pnas.191378598

Sing, A., D. Reithmeier-Rost, K. Granfors, J. Hill, A. Roggenkamp, and J. Heesemann. 2005. A hypervariable N-terminal region of *Yersinia* LcrV determines Toll-like receptor 2-mediated IL-10 induction and mouse virulence. *Proc. Natl. Acad. Sci. USA.* 102:16049–16054. doi:10.1073/pnas.0504728102

Skinner, J.A., A. Reissinger, H. Shen, and M.H. Yuk. 2004. *Bordetella* type III secretion and adenylate cyclase toxin synergize to drive dendritic cells into a semimature state. *J. Immunol.* 173:1934–1940.

Skinner, J.A., M.R. Pilione, H. Shen, E.T. Harvill, and M.H. Yuk. 2005. *Bordetella* type III secretion modulates dendritic cell migration resulting in immunosuppression and bacterial persistence. *J. Immunol.* 175:4647–4652.

Stibitz, S., W. Aaronson, D. Monack, and S. Falkow. 1989.Phase variation in *Bordetella pertussis* by frameshift mutation in a gene for a novel two-component system. *Nature.* 338:266–269.

Sun, S.C., and S.C. Ley. 2008. New insights into NF-kappaB regulation and function. *Trends Immunol.* 29:469–478. doi:10.1016/j.it.2008.07.003

Thomson, S., A.L. Clayton, C.A. Hazzalin, S. Rose, M.J. Barratt, and L.C. Mahadevan. 1999. The nucleosomal response associated with immediate-early gene induction is mediated via alternative MAP kinase cascades: MSK1 as a potential histone H3/HMG-14 kinase. *EMBO J.* 18:4779–4793. doi:10.1093/emboj/18.17.4779

Yuk, M.H., E.T. Harvill, P.A. Cotter, and J.F. Miller. 2000. Modulation of host immune responses, induction of apoptosis and inhibition of NF-kappaB activation by the *Bordetella* type III secretion system. *Mol. Microbiol.* 35:991–1004. doi:10.1046/j.1365-2958.2000.01785.x

Zhang, Z.Y. 2002. Protein tyrosine phosphatases: structure and function, substrate specificity, and inhibitor development. *Annu. Rev. Pharmacol. Toxicol.* 42:209–234. doi:10.1146/annurev.pharmtox.42.083001.144616

Milk fat globule epidermal growth factor–8 blockade triggers tumor destruction through coordinated cell-autonomous and immune-mediated mechanisms

Masahisa Jinushi,[1] Marimo Sato,[1] Akira Kanamoto,[1] Akihiko Itoh,[1] Shigenori Nagai,[2,3] Shigeo Koyasu,[2] Glenn Dranoff,[4] and Hideaki Tahara[1]

[1]Department of Surgery and Bioengineering, Advanced Clinical Research Center, Institute of Medical Science, University of Tokyo, Tokyo 108-8639, Japan
[2]Department of Microbiology and Immunology, Keio University School of Medicine, Tokyo 160-8582, Japan
[3]Core Research for Evolutional Science and Technology, Japan Science and Technology Agency, Tokyo 102-0075, Japan
[4]Department of Medical Oncology and Cancer Vaccine Center, Dana-Farber Cancer Institute and Department of Medicine, Brigham and Women's Hospital and Harvard Medical School, Boston, MA 02115

Carcinogenesis reflects the dynamic interplay of transformed cells and normal host elements, but cancer treatments typically target each compartment separately. Within the tumor microenvironment, the secreted protein milk fat globule epidermal growth factor–8 (MFG-E8) stimulates disease progression through coordinated $\alpha_v\beta_3$ integrin signaling in tumor and host cells. MFG-E8 enhances tumor cell survival, invasion, and angiogenesis, and contributes to local immune suppression. We show that systemic MFG-E8 blockade cooperates with cytotoxic chemotherapy, molecularly targeted therapy, and radiation therapy to induce destruction of various types of established mouse tumors. The combination treatments evoke extensive tumor cell apoptosis that is coupled to efficient dendritic cell cross-presentation of dying tumor cells. This linkage engenders potent antitumor effector T cells but inhibits FoxP3$^+$ T reg cells, thereby achieving long-term protective immunity. Collectively, these findings suggest that systemic MFG-E8 blockade might intensify the antitumor activities of existing therapeutic regimens through coordinated cell-autonomous and immune-mediated mechanisms.

CORRESPONDENCE
Hideaki Tahara:
tahara@ims.u-tokyo.ac.jp

Abbreviations used: 5-FU, 5-fluorouracil; BMDC, bone marrow–derived dendritic cell; MFG-E8, milk fat globule epidermal growth factor–8; NOD-SCID, nonobese diabetic–severe combined immunodeficiency; VEGFR-2, antivascular endothelial growth factor receptor–2.

Cancer pathogenesis involves not only the cell-autonomous defects that arise from alterations in oncogenes and tumor suppressors but also the impact of host antitumor responses (1). Cancer cells that have escaped immune control are selected for the ability to exploit factors present in the tumor microenvironment to further disease progression (2–4). Among this array of soluble moieties, inflammatory cytokines including TNF-α, IL-6, and IL-1β play key roles through triggering NF-κB–, STAT-3–, and MyD88-dependent pathways (5–8).

GM-CSF is another cytokine frequently produced in the tumor microenvironment, where it may contribute to either tumor protection or promotion (9). Through studies of GM-CSF–deficient mice, we identified milk fat globule epidermal growth factor–8 (MFG-E8) as a critical determinant of the pro- and antiinflammatory activities of the cytokine (10). MFG-E8 is a secreted phosphatidylserine-binding protein that signals through $\alpha_v\beta_3$ and $\alpha_v\beta_5$ integrins (9–12). Under steady-state conditions, GM-CSF induces MFG-E8 expression in mononuclear phagocytes, enabling the efficient uptake of apoptotic cells, the production of TGF-β and CCL22, and the maintenance of FoxP3$^+$ T reg cells (10). Under conditions of cellular stress, however, the ligation of Toll-like receptors dampens MFG-E8 expression, whereupon GM-CSF elicits CD4$^+$ and CD8$^+$ effector T cells through an MFG-E8–independent pathway. Thus, the levels of MFG-E8 present in the tumor microenvironment might modulate the functions of GM-CSF during carcinogenesis.

In malignant melanoma, MFG-E8 expression is increased in tumor cells and/or infiltrating

The Rockefeller University Press $30.00
J. Exp. Med. Vol. 206 No. 6 1317-1326
www.jem.org/cgi/doi/10.1084/jem.20082614

The Journal of Experimental Medicine

myeloid elements upon progression to the vertical growth phase, the stage in which melanoma cells acquire the competence for invasion and dissemination (12, 13). In a mouse melanoma model, MFG-E8 augmented tumorigenicity and metastatic capability through Akt- and Twist-dependent mechanisms (12). MFG-E8 enhanced melanoma cell resistance to apoptosis, induced an epithelial-to-mesenchymal transition, and stimulated invasion and angiogenesis. MFG-E8 also contributed to local immune suppression by evoking FoxP3$^+$ T reg cell infiltrates and suppressing Th1 reactions and NK and CD8$^+$ T cell cytotoxicity.

Because MFG-E8 is expressed at high levels in diverse tumor types (14, 15), including melanoma, this soluble protein might serve as a general target for cancer therapy. In contrast to most oncologic treatments, which primarily address either the tumor or host separately, MFG-E8 antagonists might affect both compartments. Indeed, shRNA knockdowns of MFG-E8 sensitized tumor cells to cytotoxic agents and small molecule inhibitors of receptor tyrosine kinases in vitro, whereas MFG-E8 blockade with a dominant-negative mutant potentiated tumor immunity generated with irradiated, GM-CSF–secreting tumor cell vaccines (10, 12). Based on these results, we hypothesized that systemic targeting of MFG-E8 might contribute to tumor destruction in several complementary ways. In this paper, we show that antibodies to MFG-E8 cooperate with conventional cancer therapies to effectuate sustained control of established mouse tumors through the coupling of cell-autonomous and host-mediated pathways.

RESULTS

Combinatorial therapy with systemic MFG-E8 blockade

To explore the therapeutic potential of anti–MFG-E8 antibodies, we first characterized the moderately immunogenic MC38 colon carcinoma model that is syngeneic to C57BL/6 mice. At 10 d after intradermal inoculation, when tumors were well established (~25 mm^2), the systemic administration of gemcitabine, a cytotoxic agent with modest activity in patients with colon carcinoma (16), afforded a small delay in MC38 tumor growth in a dose-dependent fashion (Fig. 1 A). Although a blocking anti–MFG-E8 mAb (17) displayed minimal antitumor activity when infused alone, combination treatment with gemcitabine resulted in tumor regressions that were sustained throughout the duration of the study (4 mo). A rabbit polyclonal anti–MFG-E8 serum (18) showed comparable efficacy (Fig. 1 B), whereas an isotype control mAb was inactive (not depicted), establishing the specificity of the response. Synergistic antitumor effects were also obtained when the anti–MFG-E8 antibodies were administered beginning 3 or 7 d after gemcitabine but not when infused before chemotherapy, indicating that the sequence of the combination was important for activity (Fig. S1).

Systemic anti–MFG-E8 antibodies similarly enhanced the therapeutic potency of 5-fluorouracil (5-FU) and CPT-11 (Fig. 1 C), two agents frequently used in the treatment of advanced colon carcinoma patients (16). As with gemcitabine, these combination therapies achieved prolonged tumor control, in contrast to the limited impact of individual agents. MFG-E8 blockade also intensified the activity of an epidermal growth factor receptor tyrosine kinase inhibitor and an antivascular endothelial growth factor receptor–2 (VEGFR-2) mAb (Fig. 1 D). Additionally, a short course of radiation therapy directed toward subcutaneous MC38 lesions was rendered more efficacious when combined with anti–MFG-E8 antibodies (Fig. 1 E). Synergistic effects of anti–MFG-E8 antibodies and chemotherapy were similarly observed in the poorly immunogenic B16 melanoma model. In this system, combinations of MFG-E8 blockade with doxorubicin, etoposide, or dacarbazine achieved significant tumor control, although gemcitabine proved inactive (Fig. 1 F and not depicted). Moreover, the combined administration of anti–MFG-E8 antibodies and doxorubicin also triggered the destruction of established EL-4 thymomas (Fig. S2). Collectively, these experiments reveal the ability of systemic MFG-E8 blockade to intensify the antitumor effects of conventional oncologic therapies in diverse tumor models.

MFG-E8 blockade enhances drug-induced apoptosis

Because standard cancer treatments displayed only modest single-agent activity against various types of tumors, we wondered whether the anti–MFG-E8 antibodies might modulate tumor cell killing. In this context, we previously showed that MFG-E8 triggered Akt activation in tumor cells through $\alpha_v\beta_3$ integrin signaling, which resulted in an attenuation of etoposide-induced death (12). In accordance with these findings, MFG-E8 was not detectable in MC38 and B16 cells at baseline, whereas cells that survived an overnight exposure to diverse chemotherapeutic drugs manifested significant MFG-E8 expression, which was evident intracellularly, at the surface membrane, and in culture supernatants (Fig. 2, A and B; and not depicted). γ irradiation also induced MFG-E8 surface expression on EL-4 thymoma (EG.7-OVA) cells (Fig. 2 C). Furthermore, stable drug-resistant variants of MC38 cells, which were generated through prolonged exposure to escalating concentrations of gemcitabine, CPT-11, or 5-FU in vitro, and similarly derived doxorubicin-resistant B16 cells demonstrated much higher levels of MFG-E8 compared with the parental tumor cells (Fig. 2 D and not depicted).

Consistent with an antiapoptotic function for surface and/or secreted MFG-E8, the addition of anti–MFG-E8 mAbs but not irrelevant control antibodies potentiated the killing of MC38 cells with gemcitabine and 5-FU, as revealed by the enhanced expression of annexin V (Fig. 2 E). The addition of rabbit polyclonal anti–MFG-E8 serum manifested comparable effects (unpublished data). The induction of apoptosis with the combined therapy also resulted in a loss of mitochondrial membrane potential (unpublished data). Moreover, the combination therapies triggered increased levels of tumor apoptosis in vivo. MC38 tumors harvested from mice that received gemcitabine plus anti–MFG-E8 antibodies showed enhanced caspase 3 activation as compared with tumors isolated from mice treated with either agent alone (Fig. 2 F). Similarly,

B16 melanomas manifested elevated caspase 3 activation after combined dacarbazine and MFG-E8 blockade. These results support the idea that MFG-E8 blockade compromises tumor cell viability in a cell-autonomous fashion, although the increased caspase activation in vivo might partially reflect the death of stromal elements within the tumor microenvironment. The anti–MFG-E8 antibodies may also attenuate tumor angiogenesis (18), which might contribute to tumor cell death as well. Collectively, these results reveal a role for MFG-E8 in mediating resistance to cytotoxic therapy and suggest that anti–MFG-E8 antibodies might serve as a complementary strategy to intensify drug-induced tumor cell killing.

Combinatorial therapy with MFG-E8 blockade stimulates T cell immunity

Because MFG-E8 plays a key role in T reg cell homeostasis (10), we investigated whether the antitumor activities of combined chemotherapy and MFG-E8 blockade might also involve host immunity. In accordance with this idea, anti–MFG-E8 antibodies failed to increase the minimal killing of MC38 cells achieved with gemcitabine in immunodeficient nonobese diabetic–severe combined immunodeficiency (NOD-SCID) mice (Fig. 3 A). Moreover, antibody depletion experiments established that $CD8^+$ and to a lesser extent $CD4^+$ T cells, but not NK cells, were required in wild-type

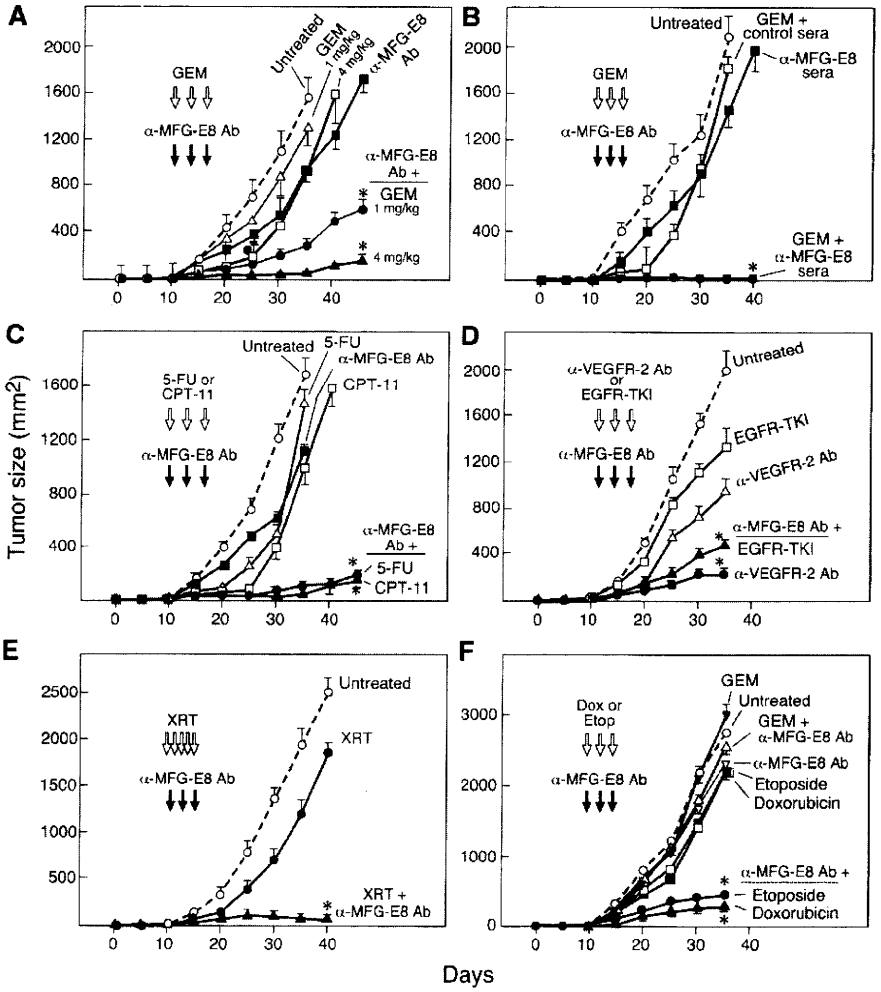

Figure 1. MFG-E8 antibody blockade synergizes with cytotoxic therapies to mediate tumor destruction. (A) Established MC38 carcinomas (25 mm^2) were treated with systemic gemcitabine (GEM) and/or an anti–MFG-E8 mAb, as indicated. (B) Same conditions as in A, but with rabbit anti–MFG-E8 sera. (C) Established MC38 carcinomas were treated with 5-FU or CPT-11 with or without anti–MFG-E8 mAb. (D) Established MC38 carcinomas were treated with anti–VEGFR-2 mAb DC101 or EGFR-TKI AG490 with or without anti–MFG-E8 mAb. (E) Established MC38 tumors were treated with local irradiation (XRT) with or without systemic anti–MFG-E8 mAb. (F) Established B16 melanomas (25 mm^2) were treated with systemic doxorubicin, etoposide, or GEM with or without anti–MFG-E8 mAb. Each experiment was performed with five mice per group, and similar results were observed for each panel in five independent experiments. Shown are the means ± SEM per cohort for a representative experiment. *, $P < 0.05$ between a treatment group and control.

mice for tumor destruction with the combination therapy, although the antitumor effects became significant compared with gemcitabine alone 40 d after combined therapy even with $CD8^+$ T cell depletion (Fig. 3 B). These findings suggest that the cell autonomous modes of tumor cell killing with MFG-E8 blockade are not sufficient to maintain durable control of the established cancers. Consistent with a key role for T cells in the generation of long-lived and specific protective immunity, treated mice rejected a subsequent lethal challenge with MC38 tumor cells but not B16 melanoma or MCA-205 fibrosarcoma cells (Fig. 3 C).

To characterize the T cell responses stimulated with treatment, we isolated tumor-infiltrating lymphocytes from regressing MC38 lesions. Although the proportions of total $CD4^+$ and $CD8^+$ T cells did not vary as a function of therapy, anti–MFG-E8 antibodies alone or in combination with CPT-11 significantly reduced the numbers of intratumoral $Foxp3^+$ T reg cells (Fig. 4 A). Although chemotherapy alone had no impact on T reg cell numbers, combined treatment with anti–MFG-E8 antibodies decreased T reg cell numbers in the spleen as well (Fig. 4 A). The T reg cells that were recovered after MFG-E8 blockade, however, did not manifest impaired function on a per cell basis, as assessed in standard in vitro suppression assays (unpublished data). These findings extend our earlier demonstration that MFG-E8 is an important determinant of antitumor T reg cell numbers (10, 12).

The combination treatment, but not anti–MFG-E8 antibodies alone, markedly increased $CD4^+$ and $CD8^+$ effector T cell activation and function. This stimulation resulted in high levels of surface CD44, IFN-γ production, and tumor-specific cytotoxicity (Fig. 4, B–D). The combination therapy also augmented the total levels of circulating IgG2a and IgG2b antibodies, which might contribute to tumor destruction through Fc-dependent cytotoxicity (Fig. S3). These results highlight the synergy between systemic MFG-E8 blockade and chemotherapy for boosting multiple antitumor effector mechanisms.

Anti–MFG-E8 antibodies enhance dendritic cell cross-presentation of tumor antigens

Because MFG-E8 promotes the uptake of apoptotic cells by mononuclear phagocytes (10, 19–21), we next characterized the impact of chemotherapy and MFG-E8 blockade on

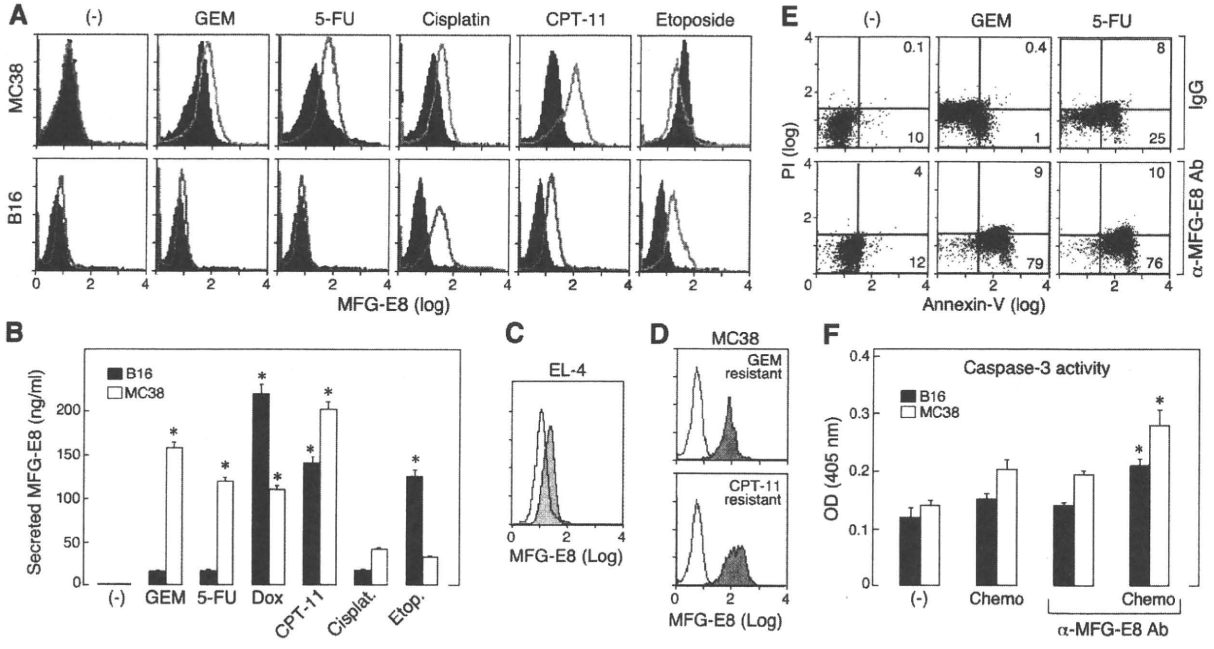

Figure 2. Drug-resistant tumor cells express MFG-E8. (A) MC38 carcinoma and B16 melanoma cells were treated with various cytotoxic agents under serum-free condition for 24 h, and intracellular MFG-E8 expression in viable cells (annexin V^-/propidium $iodide^-$) was determined with flow cytometry. The shaded and open histograms represent the levels of expression on untreated and treated cells, respectively. Gemcitabine (GEM) and 5-FU accomplished minimal killing of B16 cells (not depicted). (B) MFG-E8 levels in culture supernatants from A were measured with ELISA. (C) EL-4 thymoma cells were treated with γ irradiation (100 Gy), and MFG-E8 expression in viable cells (annexin V^-/propidium $iodide^-$) was determined with flow cytometry. (D) Stable drug-resistant variants of MC38 were generated and tested for MFG-E8 expression with flow cytometry (shaded histogram). The staining with isotype control antibodies is also shown. (E) MC38 carcinoma cells were exposed to GEM or 5-FU in the presence of anti–MFG-E8 mAb or isotype control as in A, and cell viability was determined with flow cytometry (percentages are shown). (F) Established MC38 and B16 tumors (25 mm^2) were treated with GEM or dacarbazine, respectively, with or with systemic anti–MFG-E8 mAb as in Fig. 1. 4 d after completion of therapy, tumor homogenates were prepared and assayed for caspase 3 activation with ELISA. Presented data are representative of three independent experiments with similar results. Means ± SEM are shown in B and F. *, $P < 0.05$ between the treatment and control.

antigen-presenting cells. Although the combination treatment did not influence the proportions of macrophages ($CD11b^+$ $Gr\text{-}1^-$) or myeloid-derived suppressor cells ($CD11b^+$ $Gr\text{-}1^+$) that were isolated from regressing MC38 colon tumors (Fig. S4), the numbers of $CD11b^+$, $CD11c^+$ dendritic cells were significantly increased, and these cells expressed high levels of the co-stimulatory molecule CD86 (Fig. 5 A). As bone marrow–derived dendritic cells (BMDCs) efficiently phagocytosed chemotherapy-exposed MC38 and B16 cells in vitro (Fig. S5),

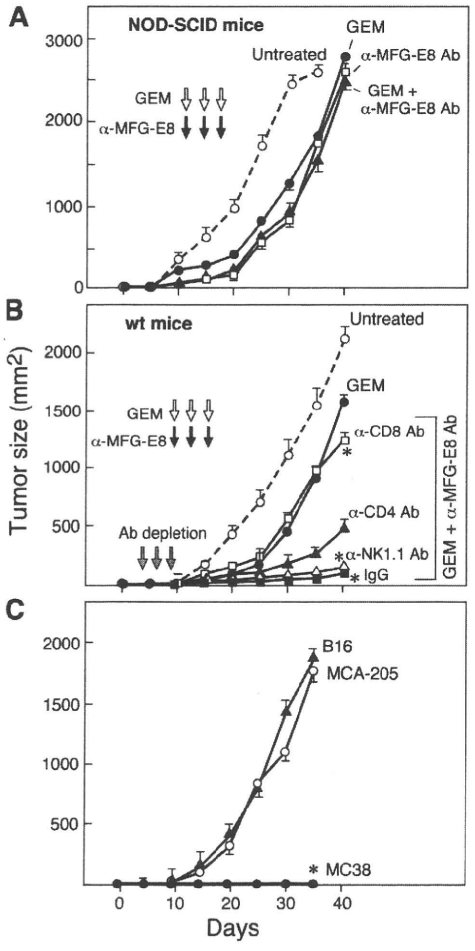

Figure 3. The therapeutic activity of MFG-E8 antibody blockade and chemotherapy involves host immunity. (A) NOD-SCID mice harboring established MC38 carcinomas (25 mm^2) were treated with systemic gemcitabine (GEM) and anti-MFG-E8 mAb. (B) Established MC38 carcinomas bearing wild-type C57BL/6 mice that were depleted of $CD4^+$, $CD8^+$, or $NK1.1^+$ cells with antibodies were treated with systemic GEM and anti-MFG-E8 mAb. (C) Wild-type C57BL/6 mice that had rejected established MC38 carcinomas with systemic GEM and anti-MFG-E8 mAb showed specific long-term protective immunity against subsequent challenge with MC38 cells during the follow-up period (>200 d). Each experiment was performed with five mice per group, and similar results were observed for each panel in three independent experiments. Shown are the means ± SEM for each cohort in a representative experiment. *, $P < 0.05$ between the treatment and control.

our analysis of the tumor infiltrates raised the possibility that dendritic cell capture of tumor cells in situ might be important for T cell priming.

To study the impact of anti–MFG-E8 antibodies on dendritic cell cross-presentation in more detail, we used EL-4 thymoma cells engineered to express OVA (EG.7-OVA) (22) and the syngeneic C57BL/6 mice harboring a transgenic TCR specific for an MHC class II–presented OVA peptide (OT-II) (23). BMDCs efficiently ingested irradiated EG.7-OVA cells, and this was only minimally blocked by an antibody to α_v integrins or MFG-E8, indicating that this pathway was not required for tumor cell uptake in this system (Fig. 5 B and not depicted). Although anti–MFG-E8 antibodies did not affect the overall phagocytosis of irradiated EG.7-OVA cells, a blocking antibody to Fc receptors but not to α_v integrins partially attenuated uptake. These results reveal that anti–MFG-E8 antibodies switch the receptor for MFG-E8–mediated tumor cell ingestion from $\alpha_v\beta_3/\alpha_v\beta_5$ integrins to Fc receptors.

Consistent with the ability of activating Fc receptors to trigger immune stimulation (24), the opsonization of EG.7-OVA cells with anti–MFG-E8 antibodies enhanced dendritic cell stimulation of OT-II TCR transgenic $CD4^+$ T cells. This activation resulted in increased production of IFN-γ (Fig. 5 C) but not IL-4 or IL-17 (not depicted). In contrast, anti-Fc receptor antibodies inhibited cross-priming, whereas anti–α_v integrin antibodies augmented T cell responses when either irradiated EG.7-OVA cells alone or anti–MFG-E8 antibody opsonized, irradiated EG.7-OVA cells were fed to dendritic cells (Fig. 5 C). The anti–MFG-E8 antibodies also increased cross-presentation to MHC class I–restricted OT-I $CD8^+$ T cells, resulting in increased IFN-γ production (Fig. S6). Collectively, these findings suggest that MFG-E8 blockade enhances Th1 antitumor responses.

To further examine the importance of MFG-E8 antibody–mediated cross-priming in vivo, we injected irradiated EG.7-OVA cells together with anti–MFG-E8 antibodies into the footpads of OT-I mice and measured OVA-specific T cell responses in the draining lymph nodes 5 d later. In some experiments, blocking anti-FcγR antibodies were coadministered to evaluate the role of FcR-mediated uptake for antigen presentation. Although the injection of anti–MFG-E8 antibodies enhanced specific $CD8^+$ T cell IFN-γ production, the concurrent administration of anti-FcγR antibodies substantially inhibited this response (Fig. 5 D). These results indicate that MFG-E8 blockade promotes cross-priming of antigen-specific $CD8^+$ T cells primarily through FcR-mediated antigen uptake.

MFG-E8 modulates dendritic cell cytokine production

To further clarify the mechanisms underlying T cell stimulation, we examined the impact of MFG-E8 on dendritic cell cytokine production after the uptake of dying tumor cells. The addition of rMFG-E8 protein increased dendritic cell IL-10 secretion, whereas anti–MFG-E8 antibodies reduced IL-10 but enhanced IL-12, IL-23, and TNF-α production (Fig. 6 A). The effects of MFG-E8 on cytokine profiles were blocked with the RMV-7 anti–α_v integrin antibody (unpublished data), confirming the importance of $\alpha_v\beta_3$ and $\alpha_v\beta_5$ integrins in this response.

To address the role of IL-12 in the immune stimulation with anti–MFG-E8 antibodies, we used IL-12p35–deficient mice in a series of in vivo and in vitro studies. The efficacy of anti–MFG-E8 antibodies and CPT-11 treatment against MC38 colon tumors was partially reduced in IL-12–deficient mice compared with wild-type controls (Fig. 6 B). Moreover, the anti–MFG-E8 antibody–mediated cross-presentation of EG.7-OVA cells to OT-II $CD4^+$ T cells was slightly decreased with IL-12–deficient dendritic cells compared with wild-type controls (Fig. 6 C). These results suggest that IL-12 contributes to the anti–MFG-E8 antibody–triggered immunostimulation, but other cytokines and/or cell-surface molecules also play important roles.

DISCUSSION

Although substantial evidence demonstrates that cross talk between tumor cells and normal host elements is critical to carcinogenesis (25), most cancer therapies primarily target individual compartments. Small molecule inhibitors of oncogenic tyrosine kinases and antibody blockade of VEGF serve as prototypes of rationally designed agents that antagonize major pathogenic mechanisms in cancer cells and the host, respectively (26, 27). Although these treatments afford important clinical benefits, most patients achieve only partial responses and eventually succumb to progressive disease caused by the emergence of drug-resistant variants. However, analogous to the ways in which antimicrobial agents cooperate with host reactions to effectuate sterilizing immunity for some serious infections (28), cancer treatments might be significantly improved through concurrently targeting the tumor and host. The results presented in this paper illustrate the potential for systemic MFG-E8 antibody blockade in combination with conventional oncologic therapies to accomplish this dual targeting.

MFG-E8 promotes cancer progression through coordinated $\alpha_v\beta_3$ integrin signaling in tumor cells, vascular elements, and infiltrating myeloid cells (12). Although the administration of anti–MFG-E8 antibodies alone resulted in only modest tumor destruction and immune stimulation, the coupling

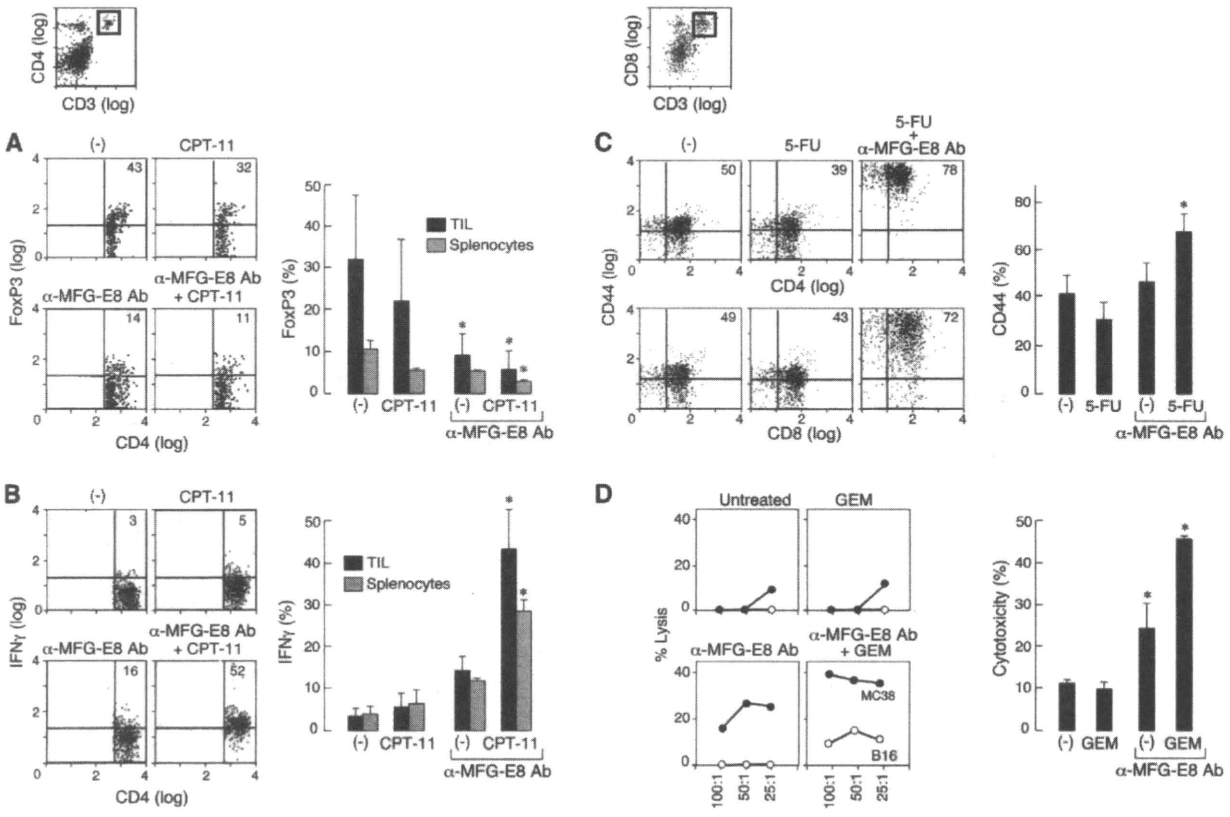

Figure 4. Combination MFG-E8 antibody blockade and chemotherapy enhances antitumor effector T cells and inhibits $FoxP3^+$ T reg cells. Tumor-infiltrating lymphocytes (TILs) were harvested from mice bearing MC38 tumors 5 d after the indicated treatment. The TILs were gated as $CD3^+CD4^+$ or $CD3^+CD8^+$ T cells, and assayed for (A) FoxP3, (B) IFN-γ, and (C) CD44 expression with flow cytometry (percentages are shown). Representative stainings are presented. The means ± SEM for six mice per group are shown in the adjacent panels. (D) Draining lymph nodes were harvested from MC38-bearing mice after the indicated treatments and evaluated for cytotoxic activity against ^{51}Cr-labeled MC38 and B16 targets in vitro. The percent specific lysis is presented. Each experiment was independently performed four times. The means ± SEM at an effector/target ratio of 100:1 for six mice per group are shown in the adjacent panels. *, $P < 0.05$ between the treatment and control.

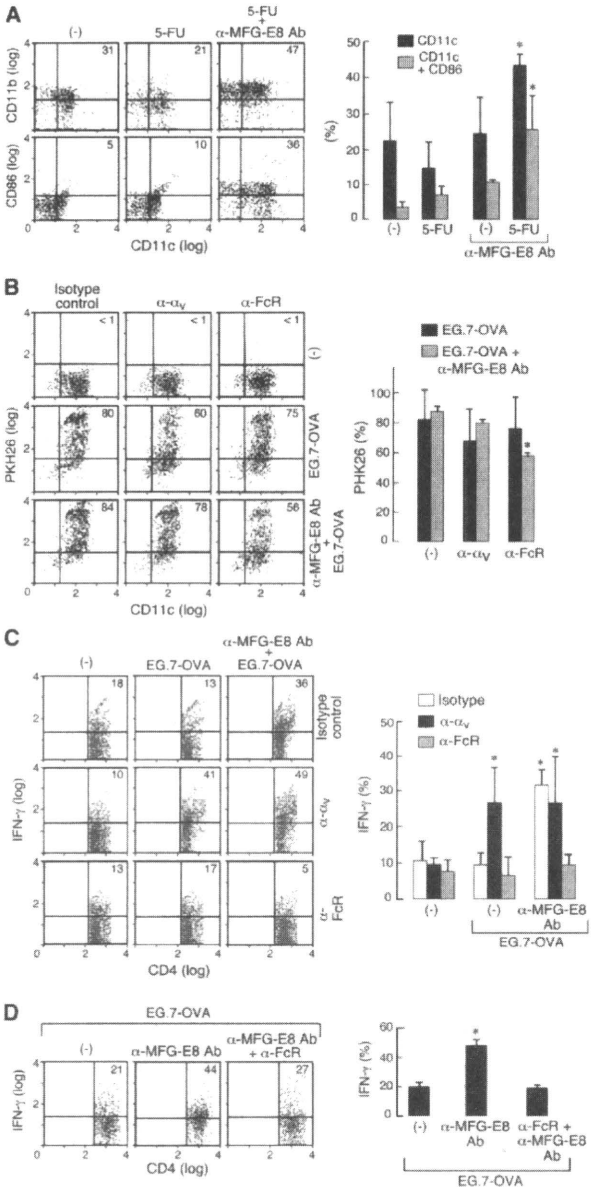

Figure 5. Anti–MFG-E8 antibodies enhance dendritic cell cross-presentation of dying tumor cells. (A) Tumor-infiltrating cells were harvested from mice harboring MC38 carcinomas 4 d after the indicated treatment. The $CD3^+$ and $B220^+$ lymphocytes were excluded by gating, and the remaining forward/side scatter high cells were analyzed for CD11c, CD11b, and CD86 with flow cytometry (percentages are shown). Similar results were observed in three experiments. Shown to the right are the means ± SEM for five mice per group. *, $P < 0.05$. (B) BMDCs were co-cultured with PKH26-labeled EG.7-OVA cells (with or without opsonization with anti–MFG-E8 mAbs) and evaluated for phagocytosis. The impact of blocking antibodies to α_v integrins and Fc receptors was determined (percentages are shown). Similar results were observed in three experiments, and the means ± SEM are shown. *, $P < 0.05$. (C) BMDCs that were loaded with EG.7-OVA cells as in B were co-cultured with OVA-specific TCR transgenic $CD4^+$ T cells, and IFN-γ production was evaluated with flow cytometry (percentages are shown). The effects of anti-α_v integrin and Fc receptor antibodies are shown. Similar results were observed in three experiments, and the means ± SEM are shown to the right. *, $P < 0.05$. (D) 10^6 irradiated EG.7-OVA cells per mouse were injected into the footpads of OT-I mice with anti–MFG-E8, anti-FcγR, and isotype control antibodies as indicated. The draining lymph nodes were harvested after 5 d, and $CD8^+$ T cell IFN-γ production was determined with flow cytometry (percentages are shown). Similar results were observed in three experiments. Shown are the means ± SEM. *, $P < 0.05$.

of drug-induced tumor cell death to MFG-E8 blockade effectuated the sustained regressions of established colon carcinomas, melanomas, and lymphomas. A key component of this therapeutic synergy is the ability of anti–MFG-E8 antibodies to attenuate tumor cell resistance to cytotoxic treatments, likely because of the inhibition of Akt activation. Some degree of intrinsic tumor cell sensitivity to the cytotoxic agent appears necessary for this enhancement, though, because gemcitabine, which failed to provoke B16 cell death in vitro (unpublished data), proved inactive in vivo in combination with MFG-E8 blockade. An additional mechanism by which anti–MFG-E8 antibodies might increase tumor cell killing, particularly in conjunction with anti–VEGFR-2 antibodies, may involve a more robust inhibition of the tumor blood supply, as MFG-E8 is required for VEGF-induced angiogenesis (14, 18). Moreover, knockdown of MFG-E8 in MC38 carcinoma cells exposed to chemotherapy also reduced VEGF production (unpublished data).

Upon the induction of tumor cell death in vivo with cytotoxic treatments, MFG-E8 blockade favored the establishment of an immunogenic tumor microenvironment. This conversion reflected the dual capacity of anti–MFG-E8 antibodies to antagonize $\alpha_v\beta_3$ integrin–driven immune suppression and to promote efficient Fc receptor–mediated dendritic cell cross-presentation. In this context, recent analysis of mice harboring a myeloid cell–specific KO of α_v integrins has underscored the importance of this receptor in attenuating inflammation (29), perhaps through the induction of Twist (12), an antagonist of the NF-κB pathway (30). Consistent with these results, we found that MFG-E8 blockade resulted in increased IL-12 production. This proinflammatory cytokine contributed to tumor protection, as revealed through studies of p35-deficient mice, although other factors such as IL-23, TNF-α, and type I IFNs may play important roles as well. Accumulating evidence has also highlighted the ability of mAbs to opsonize tumor cells for efficient cross-presentation by dendritic cells, thereby engendering potent antitumor immunity (31). Collectively, these factors may promote the development of dense intratumoral infiltrates composed of abundant $CD4^+$ and $CD8^+$ effector T cells but only limited $FoxP3^+$ T reg cells. It is tempting to speculate that this broad T cell response may suppress the emergence of drug-resistant tumor cells and mediate long-term protection against tumor recurrence. In accordance with this idea, previous experimental and clinical studies have shown that a high ratio of effector T cells to T reg cells is tightly linked with sustained tumor destruction (32, 33).